PNAS
www.pnas.org

Supplementary Information for

Climate change facilitated the early colonization of the Azores Archipelago during Medieval times.

Pedro M. Raposeiro[a,b*], Armand Hernández[c], Sergi Pla-Rabes[d], Vítor Gonçalves[a,b], Roberto Bao[e], Alberto Sáez[f], Timothy Shanahan[g], Mario Benavente[c], Erik J. de Boer[f], Nora Richter[h,i], Verónica Gordon[i], Helena Marques[a,b], Pedro M. Sousa[j,k], Martín Souto[a,b], Miguel G. Matias[l,m], Nicole Aguiar[b], Cátia Pereira[l,m], Catarina Ritter[a,b], María Jesús Rubio[c], Marina Salcedo[b], David Vázquez-Loureiro[e], Olga Margaleff[f, d, u] , Linda A. Amaral-Zettler[h,i,n], Ana Cristina Costa[a,b], Yongsong Huang[i], Jacqueline FN van Leeuwen[o], Pere Masqué[p,q,r], Ricardo Prego[s], Ana Carolina Ruiz-Fernández[t], Joan-Albert Sanchez-Cabeza[t], Ricardo Trigo[k,v], and Santiago Giralt[c]

[a] CIBIO, Centro de Investigação em Biodiversidade e Recursos Genéticos, InBIO Laboratório Associado, Pólo dos Açores, Rua da Mãe de Deus, 9500-321 Ponta Delgada, Portugal

[b] Faculdade de Ciências e Tecnologia, Universidade dos Açores, Rua da Mãe de Deus, 9500-321 Ponta Delgada, Portugal

[c] Geosciences Barcelona (Geo3BCN-CSIC), Consejo Superior de Investigaciones Científicas, Lluís Solé i Sabarís s/n, 08028 Barcelona, Spain

[d] Center for Ecological Research and Forestry Applications (CREAF), Campus de Bellaterra (UAB), Edifici C, 08193, Cerdayola del Valles, Spain

[e] Centro de Investigacións Científicas Avanzadas (CICA), Facultade de Ciencias, Campus da Zapateira s/n, Universidade da Coruña, 15071 A Coruña, Spain

[f] Department de Dinàmica de la Terra i de l'Oceà, Facultat de Ciències de la Terra, Universitat de Barcelona, Martí i Franquès s/n, 08028 Barcelona, Spain

[g] Department of Geosciences, University of Texas at Austin, Austin, TX 78712, USA

[h] Department of Marine Microbiology & Biogeochemistry, Royal Netherlands Institute for Sea Research (NIOZ), P.O. Box 59, 1790 AB Den Burg, The Netherlands

[i] Department of Earth, Environmental and Planetary Sciences, Brown University, Providence, Rhode Island 02912, United States of America

[j] Instituto Português do Mar e da Atmosfera (IPMA), 1749-077 Lisboa, Portugal

[k] Instituto Dom Luiz (IDL), Faculdade de Ciências, Universidade de Lisboa, 1749-016 Lisbon, Portugal

[l] Departmento of Biogegrafía y Cambio Global, Museo Nacional de Ciencias Naturales, CSIC, Madrid, Spain

[m] Biodiversity Research Chair - MED – Mediterranean Institute for Agriculture, Environment and Development. Universidade de Évora, Rua Dr. Joaquim Henrique da Fonseca. Casa do Cordovil, Nº7, 2º Andar. 7000-890, Évora, Portugal

[n] Department of Freshwater and Marine Ecology, Institute for Biodiversity and Ecosystem Dynamics, University of Amsterdam, The Netherlands

[o] Institute of Plant Sciences and Oeschger Center for Climate Change Research, University of Bern, Switzerland

[p] International Atomic Energy Agency, 4a Quai Antoine 1er, 98000 Principality of Monaco, Monaco

[q] Institute of Environmental Science and Technology (ICTA) and Physics Department, Universitat Autònoma de Barcelona, Bellaterra, 08193, Spain

[r] School of Natural Sciences, Centre for Marine Ecosystems Research, Edith Cowan University, Joondalup, WA 6027, Australia

[s] Department of Oceanography, Marine Research Institute (CSIC), 36208 Vigo, Spain

[t] Instituto de Ciencias del Mar y Limnología, Unidad Académica Mazatlán, Universidad Nacional Autónoma de México, 82040 Mazatlán, Mexico

[U] CSIC, Global Ecology Unit CREAF-CSIC-UAB, Cerdanyola del Vallès, 08193 Catalonia, Spain

[V] Departamento de Meteorologia, Universidade Federal do Rio de Janeiro, Rio de Janeiro

*Pedro M. Raposeiro.

Email: pedro.mv.raposeiro@uac.pt

This PDF file includes:

Supplementary text

Figures S1 to S11 (not allowed for Brief Reports)

Tables S1 to S2 (not allowed for Brief Reports)

SI References

Origin, climatology and modern ecology

The Azores Archipelago (Portugal; northeast Atlantic Ocean; 36°55–39°43N, 24°46–31°16W) consists of nine islands and several islets that are divided into three groups: the western group (Flores and Corvo), the central group (Terceira, Faial, São Jorge, Pico, and Graciosa), and the eastern group (São Miguel, Santa Maria). The archipelago spans 615 km and is located 1300 km west of Portugal and 1900 km east of North America. The ages of all islands range from 5.5 million years for Santa Maria (1) to 0.27 million years for Pico (2).

Climate

The climate of the Azores Archipelago is considered marine temperate and characterized by mild temperatures with minor annual variations. The rainfall regime displays a solid seasonal cycle and large interannual variability, high relative air humidity, and frequent strong winds (3, 4). The climatic conditions are determined by the strength and position of the Azores Current and the a semi-permanent high-pressure system known as the Azores Anticyclone (5). Most of its winter climate variability is determined by the NAO, which has its southern end on the archipelago (4, 6, 7). However, when the NAO influence becomes weaker, the effects of other large-scale climate modes of variability appear to increase, highlighting the non-stationary influence of the NAO on the Azorean climate (4, 8).

Natural vegetation

Before the human arrival, the landscape was dominated by dense laurisilva forests dominated by short-stature trees of *Juniperus brevifolia* and *Morella faya* (9–12). Throughout the centuries of human settlement, the Azores have been drastically deforested to create space for agricultural fields, supply energy for people (charcoal production), and supply raw materials for construction (13). The historical records document the practice of slash-and-burn agriculture by the first farmers (14–16). Forest areas were cut down and burned to produce charcoal, while the logged fields facilitated agriculture (14–16). The exploitation of the natural resources for local use and exportation leads to severe natural vegetation devastation. In the five centuries after the Portuguese settlement, more than 95% of Azorean natural vegetation has been destroyed (17). Currently, the vegetation of the Azores archipelago is highly degraded; lowland laurel forests are scarce and coastal woodlands are significantly reduced, and in most cases, invaded by exotic species, such as *Pittosporum undulatum* (18).

Lakes

The Azores are particularly rich in lentic habitats, with at least 88 lakes (19) located in five islands (São Miguel, Terceira, Pico and Flores and Corvo). Lakes in the Azores can be classified according to their geological setting into two main groups: (i) lakes within volcanic depressions and (ii) lakes in topographically depressed areas. The former are located in scoria cones, subsidence or collapsed calderas, or in maars. Typically, the lakes within the scoria cones are very small and shallow; lakes inside collapsed calderas show a larger surface area (Lake Azul, Lake Caldeirão), while those in maars are deeper (Lake Funda) (20). The studied lakes surface area ranges between 1.4 ha (Lake Ginjal in Terceira island) and 358.7 ha (Lake Azul in São Miguel island). Lake depth ranges between 0.5 m (Lake Ginjal) and 34.0 m depth (Lake Funda in Flores island). Lakes are located between 230 and 870 m of altitude. The Azorean lakes are subjected to several environmental pressures. Human colonization of the Azores, and the recent intensification of human activities within catchments (e.g., deforestation, agriculture, urbanization, and introduction of exotic species), has resulted in the eutrophication of many of the lakes (20–23). Azorean lakes have simple food webs and low diversity typical of remote island systems (24, 25). The natural features of these ecosystems and their small dimension within the Azorean archipelago increase its fragility and reduce the auto-regeneration ability. The main environmental gradient drivers for the biological assemblages are altitude, longitude, lake depth, and the lakes' trophic state (20, 21). Shallow lakes located at medium-high elevation (Lake Peixinho, Lake Caldeirão) are characterized by low conductivity and alkalinity, neutral to slightly acidic pH, and oligo-mesotrophic state (21). They have diverse phytoplankton communities but low biomass, dominated by desmids, chlorophytes and chrysophytes (21). Diatoms are dominated by benthic

and thycoplanktonic species belonging to the *Tabellaria*, *Brachysira*, *Encyonema* and *Frustulia* genera. The chironomid assemblages are dominated by *Micropsectra*, *Psectrocladius* and *Paratanytarsus* genus (20, 26). By contrast, deep lakes (Lake Azul, Lake Funda) are found at low elevations, present higher conductivity and alkalinity, and meso-eutrophic states (21). Phytoplankton communities present a low diversity with high biomass, dominated by cyanobacteria and diatoms. Besides the dominance of planktic diatoms (e.g., *Aulacoseira*, *Asterionella* and *Ulnaria* genera), a shift in benthic diatom assemblages towards the increase of *Achnanthidium*, *Pseudostaurosira*, *Nitzschia* and *Fragilaria* genera. Dominance of *Chironomus*, *Glypotendipes* and Psectrocladius genera in the chironomid assemblages is also observed in deep lakes (20, 21, 26).

Methods

XRF core scanner

The better-preserved half of each section of the core was analyzed using X-ray fluorescence (XRF) with the AVAATECH XRF II core scanner at the Universitat de Barcelona (Spain). Depending on the main core lithological features, the XRF measurements were performed every 2 to 5 mm, where the material was well preserved (Table S1). Among the thirty-two chemical elements measured, we only employed the iron-manganese (Fe/Mn) ratio as an indicator of the lake bottom oxygenation conditions and titanium (Ti) as a proxy for the siliciclastic inputs due to runoff.

Organic matter

Organic matter content was analyzed for all lakes (Table S1). Samples for bulk organic geochemistry were 1 cm thick, and their sampling interval varied between 1 and 5 cm, depending on the temporal resolution of the record. They were manually ground using an agate mill and analyzed for Total Carbon (TC) and Total Nitrogen (TN) (Relative standard deviation (RSD) = 5 %), and their respective stable isotopes ($\delta^{13}C_{org}$ and $\delta^{15}N_{org}$) using a Finnigan delta Plus EA-CF-IRMS spectrometer at the Centres Científics i Tecnològics at Universitat de Barcelona (CCiTUB) and a Thermo Finnigan Flash- EA1112 elemental analyser at Servizo de Apoio á Investigación at Universidade da Coruña. Previous analyses by X-ray diffraction showed negligible amounts of carbonates; consequently, TC was considered to be equal to total organic carbon (TOC). TOC and TN results are expressed as percentages of the sediment dry weight. The atomic ratio TOC/TN was calculated and corrected according to (27) to discriminate inorganically bound nitrogen content from TN. Hereafter, the TOC/TN ratio is referred to as $TOC/TN_{corr.}$ Isotopic values are reported in the conventional delta-notation (‰) relative to the Pee Dee Belemnite (PDB) carbon and atmospheric nitrogen (N_2) standards, respectively.

Palynological analyses

Palynological analyses were performed on all lake cores (Table S1). After spiking with *Lycopodium clavatum*, samples were digested with KOH, HCl, HF, and acetolysis. The residues were suspended in glycerine, and the microscopic slides were mounted in the same medium (28). Lake Azul samples were processed and analyzed at the Institute of Plant Science, University of Bern (Switzerland) and the Botanic Institute of Barcelona (IBB-CSIC, Spain), samples from Lakes Ginjal and Caldeirão were processed at the Universidade of the Azores (Portugal), and counted at the Universidade of the Azores (Portugal) and the University of Amsterdam (The Netherlands), respectively, and samples from Funda and Peixinho were processed and counted at Geosciences Barcelona (Geo3BCN-CSIC, Spain).

Identification of pollen, spores, and non-pollen palynomorphs (NPPs) was done at 400x magnification following (29–31), by comparison against the Azorean modern palynological library collection, curated by the Freshwater Ecology Research Group of the University of the Azores in

Ponta Delgada, São Miguel. Non-pollen palynomorphs (NPP) were identified according to several specialized references (32–35). Cerealia were separated from the rest of the Poaceae based on the diameter of the pollen grain (>47 μm) and the annulus (>11 μm) (36). *Zea mays* and *Secale cereale* were identified according to Beug (37). Counting followed the criteria of Rull (38), ranging from 306 to 1051 (average 580) pollen grains and pteridophyte spores per sample. The pollen sum included all identified pollen and spore types with an ecological role in the landscape, except those from aquatic and semi-aquatic taxa (Cyperaceae, *Myriophyllum,* and *Potamogeton*). A detailed interpretation of the pollen diagram from Lake Azul can be found in (39).

Micro-charcoal particles were identified and counted on the same palynological slides according to two size classes between 5 – 40 μm and > 40 μm.

Plant macrofossils

Plant macrofossil analysis was only conducted on the Lake Caldeirão core (Table S1). The samples (5 cm ^{3}) were gently washed using a sieve (125 μm mesh size) with 2 L of water. Sediment particles smaller than 125 μm were collected and left to decant in a container overnight. The screened material was transferred to Petri dishes, and plant macrofossils were separated under a stereomicroscope (10-50x). Moss leaves, Cyperaceae epidermal tissues, and small seeds were mounted into temporary slides and examined at high magnifications (100-400x). Identifications were made using a reference collection of plant parts and seed atlases (40–42) and illustrations in various publications (43–46). The macrofossil collection was stored in tubes with 70% ethanol at 4°C.

Macro-charcoal

Macroscopic charcoal analyses were conducted on contiguous 2 cm ^{3} sediment samples from Lakes Caldeirão, Peixinho, and Ginjal (Table S1). Samples were soaked in potassium hydroxide (KOH) solution (10 %) at 70°C for 30 minutes, then sieved to separate charcoal particles. These particles were counted in a Petri dish using a stereomicroscope. Charcoal concentrations (particles cm $^{-3}$) were converted to charcoal accumulation rates (CHAR, particles cm $^{-2}$ yr $^{-1}$) by multiplying each concentration by the sediment accumulation rate (cm yr $^{-1}$).

Diatoms

Diatoms were identified and counted in all lake sediment cores (Table S1). Sediment samples were processed for diatoms following standardized procedures (47). The resulting slides were mounted with a Naphrax mountant, and at least 400 valves per sample were identified and counted across random transects at 1,000x magnification using a Zeiss Axio Imager A1 microscope equipped with a 100x objective (Zeiss Plan-Apo 1.4 numeric aperture) and differential interference contrast optics. Taxonomic identification was based on general diatom floras (48–54), and compated with previous studies in the Azores archipelago (55). Taxa were grouped according to their lifestyle preferences as euplanktonic, tychoplanktonic, and benthic (56). Diatoms with aerophilic capabilities (57) were considered distinct from benthic ones and categorized in their group. Raw valve counts were converted to percentage abundance data.

Chironomids

Head capsules (HC) of chironomid larvae were identified and counted in all lake sediment cores (Table S1). They were analyzed in 2 cm ^{3} subsamples at 1 to 5 cm increments following the procedure described by (58). The samples were deflocculated in 10 % KOH, heated to 70 °C for 5 min, sieved and separated into two size fractions (90 and 212 μm). Head capsules were sorted under a stereomicroscope (40x magnification – Zeiss Stemi). HC were mounted with Euparal mounting medium and identified using a microscope at 100x – 400x magnification (ZEISS

AXIOIMAGE A1). Identification of HC was mainly based on mentum characteristics, as described in (58), and were identified to the lowest possible taxonomic resolution, usually species morphotypes, using taxonomic nomenclature (58). The relative abundance of each taxon was presented as a percentage of the total chironomid count. Chironomids were grouped according to their habitat preference (profundal, littoral, sublittoral, or free-living taxa) or oxygen tolerance (low oxygen tolerance, stable oxygen, or unstable oxygen taxa). Each taxon was classified based on recent studies on chironomid autecology (see (59) and references therein).

Sterol determination

Sterols were measured in sediment samples from Lake Funda, Lake Peixinho, Lake Caldeirão, and Lake Azul (Table S1). Lipid analysis was carried out at the University of Texas (Lake Azul) and Brown University (Lakes Funda, Caldeirão and Peixinho).

All samples were freeze-dried and homogenized before solvent extraction using a Dionex accelerated solvent extraction (ASE 350) system at 120° C and 1200 psi with dichloromethane:methanol (DCM:MeOH; 9:1 v/v). The total lipid extract was separated using silica gel flash chromatography to obtain the alkane (hexane), ketone (DCM), and polar (MeOH) fractions. The resulting ketone fraction was analyzed for sterols, stanols, and polycyclic aromatic hydrocarbons (PAHs).

Sterol and stanol samples were identified and quantified using select ion monitoring with an Agilent 7890B gas chromatography (GC) system coupled to an Agilent 5977B quadrupole mass spectrometer (MS). The samples were injected onto a ZB-1MS (30 m x 320 μm x 0.25μm) column in pulsed splitless mode (320 C, 1.3 psi). The oven temperature was increased from 40° C for 1 min to 255° C at 20° C/min and further increased to 315° C at 4 °C/min where it was held isothermally for 10 min. The ionization energy for the MS was set to 70 eV and a scan range of 50-650 m/z was used. 5-cholestan-3-one was used as an internal standard.

PAHs were analyzed with an Agilent Technologies 1200 Series high-performance liquid chromatography (HPLC) system equipped with an autosampler, binary pump feeding into a reverse-phase liquid chromatography column, diode array detector (DAD), and fluorescence detector (FLD). Before analysis, all samples were filtered using an Agilent Captiva econofilter (2 μm mesh). PAH peaks were identified via the DAD UV spectra and were then quantified using the FLD. The FLD method was constructed based on previous HPLC analysis of PAHs in lake sediments. Varying PMT-Gain adjustments were made throughout the run to ensure the appropriate magnification of peaks in the final chromatograph. The results were analyzed on Chemstation using the LC 3Dsystems software. An external calibration curve was developed using an Accustandard PAH mix consisting of naphthalene, acenaphthene, fluorene, phenanthrene, anthracene, fluoranthene, pyrene, benz[a]anthracene, chrysene, benzo[b]fluoranthene, benzo[k]fluoranthene, benzo[a]pyrene, dibenzo[a,h]anthracene, benz[ghi]pyrene, and indeno[1,2,3-cd]pyrene with concentrations varying from 50 ng mL^{-1} to 250 ng mL^{-1}. The resulting calibration curve was used to determine the final PAH concentrations.

Age-depth models for the sedimentary records

Samples for Radiocarbon AMS dating were prepared by acid digestion (60). Three plant macroremains (Lake Azul) and 40 pollen concentrated samples were analyzed at Beta Analytic Lab (USA) and Laboratoire de Radiochronologie (Université de Laval, Quebec, Canada). The AMS radiocarbon dates (Table S2) were calibrated using the Calib 7.1 software and the IntCal20 calibration curve (61). The concentration profile of ^{210}Pb was determined every centimetre for the uppermost sediments of lakes Azul, Peixinho, Caldeirão, and Funda (Table S2) through quantification of ^{210}Po by alpha-particle spectrometry, at the Autonomous University of Barcelona (Lake Azul) following (62), and at the Laboratorio de Geoquímica Isotópica y Geocronología (Instituto de Ciencias del Mar y Limnología, UNAM, Mazatlán, México) following ((63), based on (64)). Briefly, aliquots of dried ground samples, ranging from 0.08 – 0.40 g, were spiked with a

known amount of ^{209}Po yield tracer, digested with a mixture of concentrated acids ($HF+HNO_3+HCl$) at high temperature (> 120º C), and polonium isotopes were spontaneously deposited on silver discs. ^{209}Po and ^{210}Po activities were determined by alpha-particle spectrometry with high-resolution low-background Si detectors until the counting uncertainty was estimated to be < 5 %.

^{226}Ra (via ^{214}Pb) and ^{137}Cs were determined by gamma spectrometry for selected samples along the cores from lakes Funda, Peixinho, and Azul (Table S1). About 1 g of dried ground sample was placed into polyethylene calibrated geometries (length = 40 mm, diameter = 10 mm) sealed with rubber caps and Teflon tape. Samples were stored for 21 days to allow secular equilibrium between ^{226}Ra and ^{214}Pb. Samples were measured in a gamma spectrometry system with a high-resolution low-background HPGe well-type detector (Ortec-Ametek) for at least 48 hours.

The excess ^{210}Pb activities were calculated by subtracting ^{226}Ra from the total ^{210}Pb activities. Activities are reported in Bq kg $^{-1}$ and uncertainties are $\pm$ 1 sigma. Analytical quality was assured by replicate analysis of the reference material IAEA-300. Results were within the certified values for ^{210}Pb, ^{226}Ra and ^{137}Cs. $^{210}Pb_{ex}$-derived sedimentation rates were calculated by applying the Constant Flux (CF; Azul) and the Constant Flux Constant Sedimentation (CF:CS; the other cores) models (65–67). Uncertainties were calculated using Monte-Carlo with 10,000 iterations (68).

In all cases, the combined age-depth model was constructed using version 2.3.9 of the R "clam" package (69, 70). This package automatically calibrated all radiocarbon dates at 2-σ using the IntCal20 calibration curve (61).

Climate Model Simulations

To investigate the climate conditions associated with land use changes and the occupation histories of our sites, we used the Community Earth System Model (CESM-CAM5_CN) Last Millennium Ensemble (LME) transient simulation. Ensemble members extend from 851 to 2006 CE and are forced using reconstructions of changing solar intensity, volcanic emissions, greenhouse gases, aerosols, land use conditions, and orbital parameters over this time interval. The transient simulations with CESM have been used previously in a number of experiments, ranging from an assessment of continental/oceanic changes associated with recent anthropogenic forcing (71, 72), to evaluating the relative roles of internal/external forcing and their impacts on global climate (73–75). These and other previous studies have demonstrated the model performance in reproducing large-scale circulation features such as the ones analyzed in this work (74, 76).

Data is available on a 2º horizontal resolution for atmospheric data, and 36 simulations were performed for the LME project: 13 simulations with all transient forcings, smaller ensembles with each transient forcing applied separately, and long 1850 and 850 CE control simulations. The Ensemble spread was generated by using round-off differences in the initial atmospheric state. The following variables were considered in this study: mean sea level pressure (MSLP), horizontal wind at the 925 hPa level (u and v), 2 m air temperature (T), and precipitation. Estimates of temperature and precipitation for the Azores were calculated using an average of the model output in the region between (36ºN – 41ºN) and (32.5ºW - 22.5ºW). Our analysis was restricted to simulations of the period from 851-2000 CE.

The monthly MSLP time series for the extended winter (October-March) season was used to calculate the following modes of atmospheric circulation: the North Atlantic Oscillation (NAO) and the Eastern Atlantic (EA) pattern. A classical approach based on MSLP dipoles was used to calculate the indices in this study. To compute the NAO, we considered the meridional difference in average MSLP between high-latitude [60° N-70° N / 30° W-10° W] and low latitude [30° N-40° N / 30° W-10° W] sectors in the North Atlantic. A similar approach was performed for the EA, in this case consisting of the zonal difference between a west [30° N-50° N / 50° W-30° W] east [30°

N-50° N / 15° W-5° E] dipole in the northeastern Atlantic. Monthly anomalies were computed for the two dipoles relative to the 850-2000 CE climatological mean and then standardized to obtain a monthly NAO and EA series for the study period and each ensemble member. Monthly values not exceeding these thresholds were considered neutral. The typical individual and combined positive/negative anomalies in large-scale circulation and temperature (in the Euro-Atlantic sector) for NAO and EA phases during the 20th century were compared against the absolute average large-scale circulation during neutral phases, considering the Ensemble mean. Previous studies have used different definitions of the northern and southern components of the NAO and EA patterns, including station and areal averages as well as Principal Component Analysis (77, 78). Objective comparison of monthly and seasonal variability confirming the high level of similitude among these various definitions.

To obtain the combined phases of the circulation indices, we attributed positive (negative) phases of the modes when their values were above (below) 0.5 standard deviations of the series for the study period. For the analysis target period (851 – 1950 CE), the NAO and EA combinations were smoothed in time, using 10–, 30–, and 50–years filters to remove high-frequency variability and to obtain coherent circulation conditions at different time-scales. This was performed for each ensemble member.

Results

Sedimentary facies

Sediment cores were retrieved from five different lakes and the resulting composite cores vary in length and composition depending on the depositional environment and catchment area of the lake.

Lake Caldeirão

The sedimentary sequence from Lake Caldeirão (460 cm in length) is dominated by reddish-brown mud and plant fragments that were deposited under shallow lacustrine conditions. The mud facies overly thick tephra deposits (fine ash) that likely originated from cinder cones visible at the bottom of the present-day lake (Fig. S1).

Lake Funda

The sediment record from Lake Funda is 994 cm in length. The lower section of the core (368-994 cm) consists of brown to black organic-rich mud and plant remains that is interbedded with sand and gravel layers containing fragments of wood (Fig. S2). The uppermost section of the core (0-368 cm) is laminated with alternating layers of brown mud and yellow diatom oozes.

Lake Peixinho

The record retrieved from Lake Peixinho is 253 cm in length and overlies coarse-grained alluvial deposits. The lacustrine sediment is composed of massive brown to black mud and plant remains that were likely deposited under shallow lacustrine conditions (Fig. S3). Tephra layers (lapilli) were identified at 205-210 cm and 175-197 cm.

Lake Ginjal

The sediment core from Lake Ginjal (350 cm) consists of a tephra layer at 280-350 cm overlain by brown mud with plant remins in the uppermost 280 cm (Fig. S4).

Lake Azul

The original sediment record for Lake Azul was previously published and described in detail (39, 79). Briefly, the lowermost section of the core contains 2 m of compact, pumiceous, and gravelly tephra (lapilli). Between 116-150 cm the sediment is composed of alternating tephra deposits and silty-grey mud (Fig. S5). From 77-116 cm the sediment transistions to silty-brown mud that is rich in particles of volcanic glass. The uppermost 77 cm consist of brown mud interbedded with thin, turbidite-like layers that are rich in sand grains and terrestrial plant remains.

Record chronologies

All age-depth models were developed in R using the version 2.3.9 of the R Clam package (69, 70, 80). This package automatically calibrated all radiocarbon dates at 2-σ using the IntCal20 calibration curve (61).

Lake Caldeirão

The age-depth model was developed using nine ^{14}C dates (Table S2) and a ^{210}Pb profile that spans the uppermost 20 cm (Fig. S6). All samples were taken from the CL1703 core, except two samples at 110 cm and 190 cm depth that were taken from the CL19-02G gravity core, which was lithologically correlated to CL1703. The resulting age-depth model spans the last 4,000 years. The period from [500-1950 CE] studied in this manuscript has a sedimentation rate of ca. 0.6 mm yr $^{-1}$ and the confidence interval for the Lake Caldeirão age-depth model ranges between 1.5 and 124 years.

Lake Funda

The age-depth model for Lake Funda was constructed using six ^{14}C dates (Table S2) and ^{210}Pb and ^{137}Cs profiles for the uppermost 74 cm (Fig. S4). Radiocarbon samples taken at 162, 168, 624 and 992 cm were discarded as they were located near allochthonous and coarse terrigenous sediments, resulting in the incorporation of old organic matter. The radiocarbon sample at 60.8 cm was also removed from the age-model as it was inconsistent with results from the ^{210}Pb and ^{137}Cs profiles. A linear interpolation was used to generate the age-depth model after removing slump events that were identified by coarse allochthonous and terrigenous material in the sediment record. The final age-depth model spans c. 720 years over 798 cm of sediment. The sedimentation rate decreases from ca. 7.3 mm yr $^{-1}$ in the lower section of the sediment record (368-994 cm) to ca. 5.2 mm yr $^{-1}$ in the uppermost section of the core (0-368 cm). The confidence interval for the Lake Funda age-depth model ranges between 1 and 50 years.

Lake Peixinho

For Lake Peixinho the age-depth model was developed with four ^{14}C dates (Table S2) and ^{210}Pb and ^{137}Cs profiles that span the uppermost 18 cm (Fig. S6). This model was constructed using a locally weighted spline (loess) with a smoothing factor of 0.1 after removing two lapilli tephra layers and a mass-wasting event between 18 and 47.5 cm. The radiocarbon date at 47.6 cm was removed from the final age-depth model due to its inconsistency with the ^{210}Pb dates and likely contamination from a mass-wasting event. The resulting age-depth model spans the last c. 690 years with sedimentation rates of 0.3 mm yr $^{-1}$ from 216 to 212 cm, which increase to ca. 6 mm yr $^{-1}$ on 205 cm and increase again to 7.9 mm yr $^{-1}$ and 10.2 mm yr $^{-1}$ 126 and 86 cm, respectively. The confidence interval for the Lake Peixinho age-depth model ranges between 1 and 112 years.

Lake Ginjal

The age-depth model for Lake Ginjal uses three ^{14}C dates and was generated using a smooth spline (Table S2; Fig. S6). Radiocarbon dates sampled at 40.0-42.5 and 237.5-240.0 cm were not included in the model because they were older than the stratigraphically adjacent dates. The resulting age-depth model spans c. 600 years from 1400-1950 CE with a sedimentation rate ranging from 25 mm yr $^{-1}$ (275 cm) to 2.7 mm yr $^{-1}$ (175 cm). The confidence interval for the Lake Ginjal age-depth model ranges between 10 and 110 years.

Lake Azul

The chronological model for Lake Azul was constructed using two ^{14}C dates and ^{210}Pb and ^{137}Cs profiles that span the uppermost 74 cm of the sediment record (Fig. S6). The age-depth model was previously published (39, 79) without the ^{210}Pb and ^{137}Cs data. Based on the ^{210}Pb profile from core AZ11-14, the previously published record from core AZ11-02 was missing the uppermost 19 cm and not 30 cm (79). The ^{14}C age at 82.8 cm was inconsistent with the results from the ^{210}Pb profile and therefore was excluded from the final age model. After removing four turbidite-like layers from the sediment record, the final age-depth model was constructed using a smooth spline method with 0.6 smoothing. The resulting age model spans the last ca. 700 years with a confidence interval for the age-depth model that ranges between 1.4 and 223 years.

Environmental and climatic evolution of Lakes Caldeirão, Funda, Peixinho, Ginjal, and Azul

Lake Caldeirão (Corvo Island)

Phase I (500-700 CE)

From 500-700 CE there are very few changes in the proxy-based records. About 85% of the pollen record is dominated by arboreal pollen and shrubs, particularly *Juniperus brevifolia*, *Ilex perado*, and *Myrsine africana* shrubs. The remaining pollen is derived from mosses and larger ferns (*Culcita macrocarpa* and *Dryopteris azorica*) (Fig. S1). A mean TOC/TN ratio of 18.4$\pm$0.4 (Fig. S7A) and δ^{15}N values between 6.8 and 7.1 ‰, suggest that organic matter in the sediment record is primarily derived from allochthonous sources (81, 82). Ti values are lower in this section of the sediment record relative to Phases II and III (Fig. S1). Biological assemblages are dominated by benthic diatom taxa, such as *Staurosira* spp. and *Stauroforma* spp., and sublittoral and oligotrophic Chironomidae taxa (*Micropsectra* spp.), indicating low levels of productivity within the lake (83, 84). The Fe/Mn ratio also remains low, indicating that the lake bottom water remained oxic (85). Polycyclic aromatic hydrocarbons (PAHs), macro-charcoal particles (diameter >125 μm), spores from coprophilous fungi, and 5β-stigmastanol are largely absent in this section of the sediment record.

Phase II: 700 – 1070 CE

This period is marked by distinct changes in proxies derived from the terrestrial environment. First, with the increase of PAHs after c. 700 CE (total flux < 6 ng cm $^{-2}$ yr $^{-1}$) and the first evidence of 5β-stigmastanol (total flux < 2 ng cm $^{-2}$ yr $^{-1}$ around 750 CE and 820 CE). Macro-charcoal is present in the sediment record after c. 850 CE (3.7 fragments cm $^{-2}$ yr $^{-1}$) and the first evidence of coprophilous fungi, around 880 CE. Although there are no major changes in the pollen record, the flux of *Juniperus* macrorests increases from 0.3 to 2.3 leaves cm $^{-2}$ yr $^{-1}$ after ca. 720 CE (Fig. S1). In contrast, there are no distinct changes in the macrophyte, diatom, and chironomid assemblages or in the bulk organic matter composition.

Phase III: 1070 – 1450 CE

The onset of this phase is marked by coincident increases in the sedimentation rate (ca. 11 mm yr $^{-1}$), 5β-stigmastanol (0.14 µg cm $^{-2}$ yr $^{-1}$), PAHs, and macro-charcoal (Fig. S1). This is followed by peaks in macro-charcoal particle inputs (maximum of 28.0 fragments cm $^{-2}$ yr $^{-1}$), PAH fluxes (increase from 3.0×10 ^{5} to 1.1×10 ^{6} ng cm $^{-2}$ yr $^{-1}$), *Juniperus* leaves (maximum value 35.1 leaves cm $^{-2}$ yr $^{-1}$), and macrophyte fluxes (maximum value 31.0 seeds cm $^{-2}$ yr $^{-1}$) ca. 1280 CE. These changes are followed by an increase in δ^{15}N 9.1 ‰, and a decrease in TOC/TN (from 19.3 to 15.9) around ca. 1280 CE. In the biological assemblages, aerophilic diatom taxa (*Humidophila* spp.: 16 %) increase and the unique occurrence of the planktonic *Fragilaria tenera* is observed. Similarly, the relative abundance of profundal chironomid taxa increases from 7.6$\pm$1.1 to 14.4$\pm$2.6 % (e.g. *Chironomus* spp.).

Phase IV: 1450 – 1950 CE

The beginning of this phase (ca. 1550 CE) is marked by a decrease of arboreal pollen from 27.1 to 17.8 %, an increase in macrophyte inputs (1.8 seeds cm $^{-2}$ yr $^{-1}$), and the disappearance of *Juniperus* leaves from the sediment record. Further, this time period is marked by the first appearance of *Aphanes*, an introduced plant species, in the pollen record. The chironomid assemblages also change ca. 1550 CE from sublittoral to predominantly littoral taxa. Coprophilous fungal spores also increase from 0.04 to 0.20 spores cm ^{2} yr $^{-1}$ after c. 1550 CE and the influx of 5β-stigmastanol sporadically increases throughout this phase. TOC, TOC/TN, and δ^{13}C values increase throughout this phase, whereas δ^{15}N values decrease ca. 1680 CE from 7.6 to 4.7 ‰. In the diatom record, mesotrophic diatom species, such as *Nitzschia* spp., increase during this phase, whereas tychoplanktonic diatoms (i.e., *Staurosira* spp. and *Punctastriata* sp.) decrease. During this phase, we also observe opportunistic diatoms like *Achnanthidium minutissimum* (79).

Lake Funda (Flores Island)

Phase II: ca. 950 CE to 1070 CE

This section of the core is characterized by organic rich mud interbedded with gravel and sand layers (Fig. S2). The pollen record consists of about 75 % arboreal pollen, namely *Laurus azorica, Juniperus brevifloria,* and *Picconia azorica*, and 10 % shrubs, including *Myrsine*, *Culcita macrocarpa,* and *Pteris incompleta*. Coprophilous fungal spores and 5β-stigmastanol are absent in this section of the record. The TOC/TN ratio remains stable at 18.3$\pm$0.4, while δ^{15}N fluctuates between 2.6 and 6.3 ‰ (Fig. S2 and Fig. S7). The diatom assemblage is dominated by mesotrophic benthic taxa, such as *Navicula* spp. and *Psectrocladius* spp., and small tychoplanktonic diatom taxa (i.e., *Pseudostaurosira* spp. or *Staurosirella* spp.). Similarly, the chironomid assemblage primarily consists of species that are found in the profundal zone and tolerate low oxygen conditions, such as *Chironomus* spp.

Therefore, the changes in regional indicators, such as the large increase in micro-charcoal influx up to 3,024 particles cm $^{-2}$ yr $^{-1}$ ca. 1150 CE and the drop in arboreal pollen from 77.2 to 53.8 %, the rise of shrubs from 12.6 to 30.9 %.

Phase III: 1070 - 1450 CE

The onset of this phase is marked by the first appearance of coprophilous fungal spores (e.g., *Sporormiella*) ca. 1330 followed by a peak in macro-charcoal particles (840$\pm$48 particles cm ^{2} yr $^{-1}$) ca. 1400 CE and a decline in arboreal pollen from 75.2$\pm$2.1 to 54.9$\pm$9.3 % ca. 1420 CE (Fig. S2). The sedimentation rate increases from 9.4$\pm$0.8 to 12.2$\pm$1.0 mm yr $^{-1}$ at the start of this phase. This is followed by a rapid increase in the macrophyte influx with a maximum of 5022 seeds cm ^{2} yr $^{-1}$ ca. 1380 CE. These changes are coincident with a depletion of δ^{15}N from 3.8$\pm$0.44 to 3.3$\pm$0.2 ‰, a decrease in the TOC/TN ratio from 18.9$\pm$0.4 to 12.9$\pm$0.3 %, and a rise in mesotrophic and euplanktonic diatom species, namely *Aulacoseira granulata* and *Aulacoseira ambigua*. Further the abundance of chironomid head capsusles, in particular macrophyte associated taxa, increases from 5.6$\pm$1.0 to 9.9$\pm$1.9 head capsules cm ^{2} yr $^{-1}$, whereas low oxygen tolerant taxa (*Chironomus* spp.) decrease.

Phase IV: 1450 CE to 1950 CE

The final phase is marked by a further decline in arboreal pollen from 37.5 to 29.6 % and the first detection of 5β-stigmastanol (4.04 µg cm ^{2} yr $^{-1}$) ca. 1500 CE. The influx of coprophilous fungal spores remains constant throughout this time period (mean value about 467 spores cm ^{2} yr $^{-1}$). This time period is also marked by the first appearance of coprostanol ca. 1625 CE in the sediment record. The sediment record also transitions from dark brown and organic rich mud to massive, brown and silty mud that is dominated by planktonic diatoms such as *Aulacoseira* spp. (>85 % of the diatom assemblage) ca. 1500 CE. δ^{15}N values also decline from 3.3$\pm$0.2 to

2.0±0.2 ‰, while Fe/Mn increases ca. 1600 CE. δ^{13}C values gradually decrease, whereas the TOC/TN ratio remains stable at 1700 CE.

Lake Peixinho (Pico Island)

Phase I (500-700 CE)

After ca. 690 CE, the pollen record shows a reduction in tree cover. The mean TOC/TN ratio remains around 18.6±0.4 and δ^{15}N values remain around 2.8‰. The diatoms assemblage was dominated by oligotrophic benthic species, including the *Eunotia incisa* and *Eunotia rhomboidea* (79). The chironomid record was primarily composed of free-living chironomids, such as Tanypodinae (26, 83).

Phase II: 700 – 1070 CE

5β-stigmastanol was measured around ca. 700 CE. After c. 850 CE, 5β-stigmastanol and PAHs are continously present in low abundance (Fig. S3) and coprostanol is absent. This is coincident with a small increase in macro-charcoal accumulation rates and a large, but brief, increase of allochthonous aerophilic diatoms (reaching 23.4 % of the diatom assemblage). This phase is also marked by the rise of mesotrophic tychoplanktonic diatoms, such as *Pseudostaurosira brevistriata*, and chironomids typically found in the profundal zone and under low oxygen conditions (e.g. *Chironomus* spp.). δ^{15}N values also decrease from 2.8±0.4 to 1.9±0.4 ‰.

Phase III: 1070 – 1450 CE

This phase is marked by the first occurrence of coprostanol (0.01 µg cm ^{2} yr $^{-1}$) ca. 1070 CE. The start of this phase is marked by a peak in 5β-stigmastanol (0.17 µg cm $^{-2}$ yr $^{-1}$) and coprostanol (0.04 µg cm $^{-2}$ yr $^{-1}$) at ca. 1120 CE (Fig. S3) and marked by the first evidence of coprophilous fungi. The initial increase in stanols is followed by a decrease in arboreal pollen from 77.1 to 54.0 % at ca. 1150 CE and a corresponding increase in the relative abundance of herbs from 19.0 to 34.5 %. After ca. 1330 CE the relative abundance of woody vegetation decreases again from 37.9 to 31.0 %, whereas herbaceious plants increase slightly from 53.9 to 56.3 %. A reappearance of *Secale cereale* occurs ca. 1200 CE, coinciding with an increase of *Plantago* spp. to 6.2 %. This phase is also associated with an increase in the sedimentation rate from from 0.8±0.1 to 3.3±0.6 mm yr $^{-1}$. Macrocharcoal inputs to the sediment remain relatively low except for a small peak at ca. 1120 CE and a larger peak at ca. 1330 CE (15.7 particles cm ^{2} yr $^{-1}$). The flux of PAHs remains relatively constant (around 3 µg cm ^{2} yr $^{-1}$) throughout this phase, except for two peaks at ca. 1120 CE (7.18 µg cm ^{2} yr $^{-1}$) and ca. 1330 CE (8.64 µg cm $^{-2}$ yr $^{-1}$).

There are few changes in the diatom and chironomid assemblages between 1120 and 1330 CE. The relative abundance of aerophilic diatoms gradually increases during this phase, mainly associated with an increase in *Humidophila* spp. and *Karayevia* spp. After 1330 CE, however, there is an abrupt increase in meso-eutrophic planktonic diatoms, including *Aulacoseira* spp., and a decrease of free-living chironomids, namely *Tanypodinae* sp. In contrast, the macrophyte flux increases throughout this phase with a peak of 65.75*10 ^{3} seeds cm $^{-2}$ yr $^{-1}$ ca. 1330 CE. During this phase both TOC/TN and δ^{15}N values remain around constant at 14.7±0.1 2.5±0.3 ‰, respectively. Finally, there is an increase in Fe/Mn values from 80 to 164 throughout this phase.

Lake Ginjal (Terceira Island)

Phase IV: 1450 CE to 1950 CE

The pollen record is dominated by herbaceous plants (>90 %), namely *Poaceae* and *Plantago* spp., and a low abundance of pollen from trees (1.2±0.3 %) and shrubs (5.0±1.5 %) (Fig. S4). Native tree species are completely absent from this sedimentary sequence, whereas *Cerealia* sp. is detected in four different samples. Throughout this record the influx of corpophilous fungal spores (20.9±14.3 spores cm $^{-2}$ yr $^{-1}$) and macro-charcoal particles (15.5 fragments cm $^{-2}$ yr $^{-1}$) remains elevated. The diatom assemblage includes aerophilic diatoms, such as *Pinnularia*

borealis s.l., and diatoms found under eutrophic conditions like *Fragilaria tenera*. After c. 1450 CE there is a sharp increase in meso-eutrophic tychoplanktonic diatoms, such as *Tabellaria flocculosa*, and in macrophyte associated taxa, such as *Paratanytarsus* sp. The chironomid assemblage is primarily composed of species found under low oxygen conditions (e.g. *Chironomus* spp.). The TOC/TN ratio remains low throughout this record (11.3±0.05), whereas δ^{15}N gradually becomes more depleted, decreasing from 3.5±0.3 to 2.1±0.9 ‰ (Fig. S4 & S7d).

Lake Azul (São Miguel Island)

Phase III: 1280 – 1450 CE

The start of phase B in Lake Azul is marked by multiple tephra layers ca. 1280 CE (Fig. S5). These layers are followed by a sharp decline in aerophilic diatoms and a decline in Ti counts. The rest of phase B is dominated by benthic and opportunistic diatoms, including *Achnanthidium minutissimum* s.l. The pollen record is characterized by a decrease in arboreal pollen, in particular laurisilva, from ca. 60 to 20 % and an increase in pollen derived form shrubs. *Secale cereale* is also observed during this phase from ca. 1280-1350 CE. Coprophilous fungal spores, coprostanol, and 5β-stigmastanol are present throughout this record. This section of the sediment core also contains elevated charcoal counts, TOC/TN values around 8.8$\pm$0.2, and δ^{13}C values around -24.92$\pm$1.98 ‰ (Fig. S7e).

Phase IV: 1450 CE to 1950 CE

Native shrubs and grasses dominate the pollen record during phase C, whereas only ca. 20% of the record is composed of arboreal pollen. TOC gradually increases from 0.61 to 1.43 % and TOC/TN values increase from 8.6 to 10.3. Both δ^{15}N and δ^{13}C becoming gradually more depleted during this phase with values decreasing from 2.5 to 1.2 ‰ and -24.1 to -25.6 ‰, respectively. In the diatom assemblage *Nitzschia* spp. and *Aulacoseira* spp. are both observed, which are found in under non-N limiting and eutrophic conditions, respectively (79).

Simulations

Simulations of Mean Sea Level Pressure (MSLP), 2 m temperature, and 925 hPa horizontal wind for combinations of NAO/EA phases during the period between 850-1950 CE (Fig. S8) display very similar results to the combinations of NAO/EA phases for the last century (Fig. S9). Combined positive NAO and EA phases (Fig. S10) resulted in lower-than-average temperatures over Iceland, Greenland, and North Africa, whereas the United Kingdom, Scandinavia, and the eastern North Atlantic (including the Azores Archipelago) experienced higher-than-average temperatures. Two higher-than-normal MSLP centers were present over continental Europe and North America, and lower-than-average MSLP values occurred between 60 - 70 °N of the North Atlantic Ocean. This combination triggered wind field anomalies over the southeast and northwest Atlantic and a northernward migration of the westerlies.

Combined positive NAO and negative EA phases (Fig. S10) resulted in lower-than-average temperatures over Greenland, eastern North America, and the central Atlantic (45 – 60 °N by 15 – 45 °W). Conversely, Iceland, most of continental Europe, North Africa, and the mid-latitudes (30 – 45 °W) of the western Atlantic experienced higher-than-average temperatures. Low MSLP values occurred over Iceland and the British Isles, whereas high MSLP values were centered over the westernmost part of the Azores Archipelago. This atmospheric configuration resulted in enhanced westerly winds between 45 – 60 °N with a slightly enhanced northerly component.

Combined negative NAO and positive EA phases (Fig. S10) resulted in lower-than-average temperatures over eastern Europe and the mid-latitudes (30 – 45 °W) of the western Atlantic. In contrast, higher-than-average temperatures were observed over Greenland, eastern North America, and the central Atlantic. This NAO/EA combination triggered an MSLP dipole with higher-than-average MSLP values over Iceland and lower-than-average MSLP values over the

central Atlantic. These MSLP anomalies gave rise to a southern migration of the westerlies (< 30 °N), resulting in weakened westerlies between 35 and 60 °N.

Combined negative NAO and EA phases (Fig. S10) resulted in lower-than-average temperatures over continental western and northern Europe and higher-than-average temperatures over the North Atlantic with maximum temperatures occurring in Iceland and Greenland. Similarly, MSLP anomalies were lower-than-average over Europe and higher-than-average over the North Atlantic. This pattern led to weakened westerly winds over the North Atlantic (25 – 65 °N) sector and enhanced northerly winds from Scandinavia to the Iberian Peninsula.

Phase II: 850- 1070 CE

Before ca. 900 CE, negative NAO phases were more frequent. During NAO $^{-}$/EA $^{+}$ and NAO $^{-}$/EA $^{-}$ phases temperatures were higher-than-average and lower-than-average, respectively, and the westerlies were weakened over the Azores Archipelago. Similar conditions occurred during NAO $^{-}$/EA $^{-}$phases, but with an enhanced northerly wind over the Azores (Fig. S8 and Fig.S11).

Phase II roughly coincides with the Medieval Climate Anomaly (MCA), which is usually defined as a warmer-than-average period in the Northern Hemisphere (86). Our results from climate model simulations show higher-than-average temperatures at 900. Drier conditions occur in the Azores ca. 940-960 CE and 1070-1080 CE. Periods with prevalent NAO $^{+}$/EA $^{+}$ phases occurred at approximately 900, 950, 1030 CE, whereas NAO $^{+}$/EA $^{-}$ phases are observed at 930, 960, 1010, 1020 and 1070 CE. NAO $^{-}$/EA $^{-}$ phases are observed at 990-1000 CE (Fig. S8).

Phase III: 1070 – 1450 CE

Phase III corresponds to the transition between the MCA and the Little Ice Age (MCA-LIA) as well as the first 50 years of the LIA. The simulated precipitation suggests three cold events centered around 1180 CE, 1210 CE, between 1260 and 1300 CE; and that the Azores experienced wetter conditions between 1350-1450 CE. This coincides with a NAO $^{+}$/EA $^{-}$ phase between 1340-1380 CE, NAO $^{-}$/EA $^{+}$ phases at 1430-1460 CE and 1490 CE, and NAO $^{-}$/EA $^{-}$ phases at ca. 1110, 1180, 1210, 1270, 1420 and 1470 CE (Fig. S8). Between ca. 1430-1490 CE, temperatures dropped below average for this time period and NAO phases were more frequent. This was associated with weakened westerlies over the Azores Archipelago, and enhanced northerly winds during NAO $^{-}$/EA $^{-}$ phases.

Phase IV: > 1450 CE

Phase IV spans the LIA, which is usually defined by colder-than-average temperatures in the Northern Hemisphere. Results from the model simulations show that temperatures were above average between 1500-1600 CE and generally remained below average between 1600-1800 CE in the Azores Archipelago. Distinct cold periods are observed between 1700-1730 CE and 1750-1770 CE. There are few variations in the simulated precipitation with the exception of three dry intervals centered c. 1500-1520 CE, 1670-1690 CE, and 1770 CE. This is coincident with more frequent negative NAO phases. Positive EA phases dominate th 18th century, with a short interval of more frequent negtive EA phases between c. 1720-1730 CE (Fig. S8).

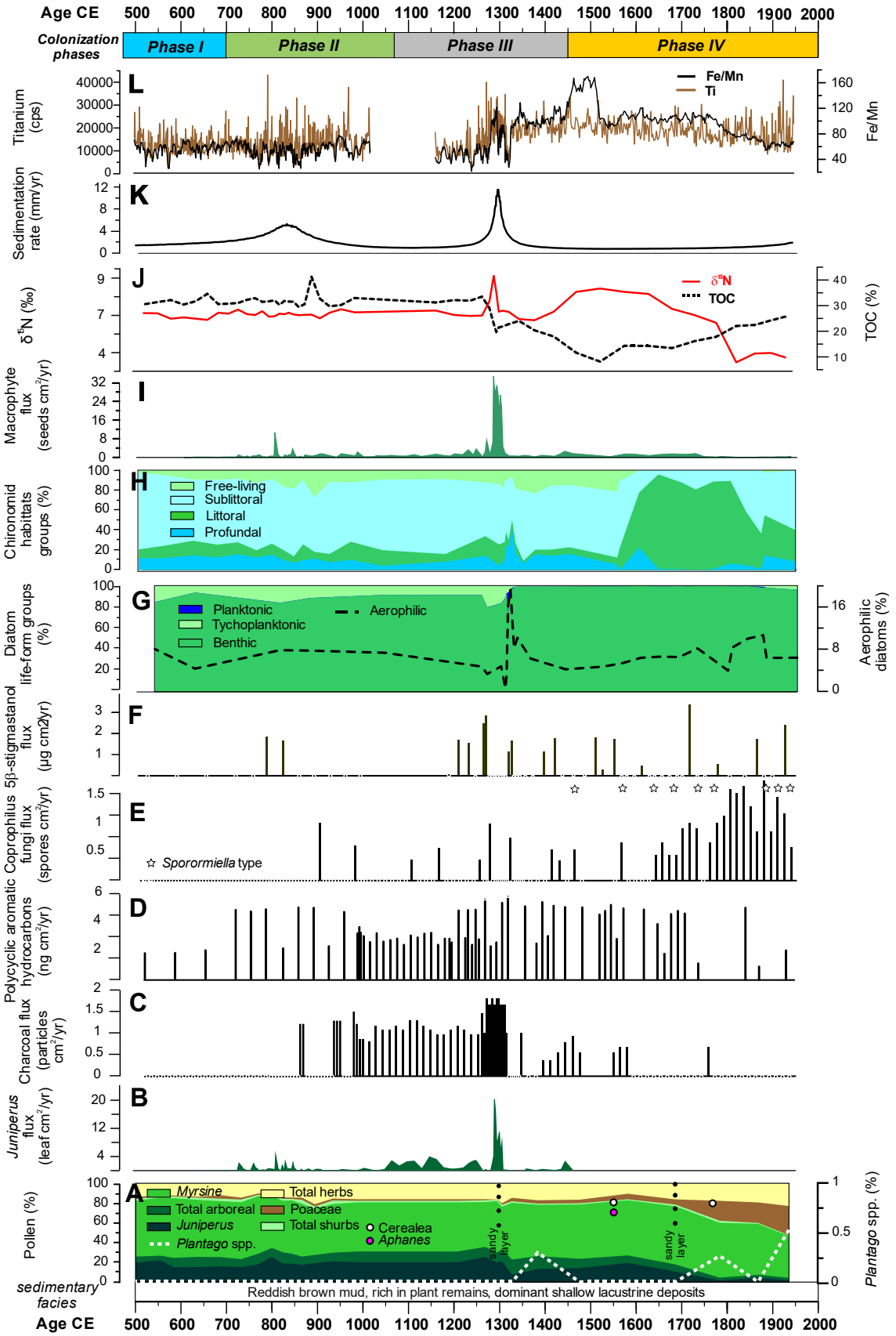
Age CE
500 600 700 800 900 1000 1100 1200 1300 1400 1500 1600 1700 1800 1900 2000
Colonization phases
Phase I
Phase II
Phase III
Phase IV
L
Titanium (cps)
Fe/Mn
Ti
Fe/Mn
K
Sedimentation rate (mm/yr)
J
δ15N (‰)
δ15N
TOC
TOC (%)
I
Macrophyte flux (seeds cm2/yr)
H
Chironomid habitats groups (%)
Free-living
Sublittoral
Littoral
Profundal
G
Diatom life-form groups (%)
Planktonic
Tychoplanktonic
Benthic
Aerophilic
Aerophilic diatoms (%)
F
5β-stigmastanol flux (µg cm2/yr)
E
Coprophilus fungi flux (spores cm2/yr)
Sporormiella type
D
Polycyclic aromatic hydrocarbons (ng cm2/yr)
C
Charcoal flux (particles cm2/yr)
B
Juniperus flux (leaf cm2/yr)
A
Pollen (%)
Myrsine
Total herbs
Total arboreal
Poaceae
Juniperus
Total shurbs
Cerealea
Aphanes
Plantago spp.
sandy layer
sandy layer
Plantago spp. (%)
sedimentary facies
Reddish brown mud, rich in plant remains, dominant shallow lacustrine deposits

Fig. S1. Environmental evolution of Lake Caldeirão (Corvo Island) from 500 to 1950 CE. A) Pollen (%); B) Juniperus flux (leaf. $cm^{-2}.y^{-1}$); C) Charcoal flux (particles. $cm^{-2}.y^{-1}$); D) Total pyrolytic PAHs flux (ng. $cm^{-2}.y^{-1}$); E) Coprophilous fungi flux (spores. $cm^{-2}.y^{-1}$); F) Fecal sterol biomarkers 5β-stigmastanol flux (µg. $cm^{-2}.y^{-1}$) and coprostanol (5β-cholestan-3β-ol) G) Diatom life-forms groups (%) and aerophilic diatoms (%); H) Chironomid habitat associated (%) and chironomid head capsule flux ($cm^{-2}.y^{-1}$); I) Macrophyte influx (seeds $cm^{-2}.y^{-1}$) J) Nitrogen stable isotopes – δ15N (‰) and Total organic content – TOC (%); K) sedimentation rate ($mm\text{-}^{1}.y^{-1}$); L) Titatium (cps) and Fe/Mn ratio. Phases explanation (see main manuscript).

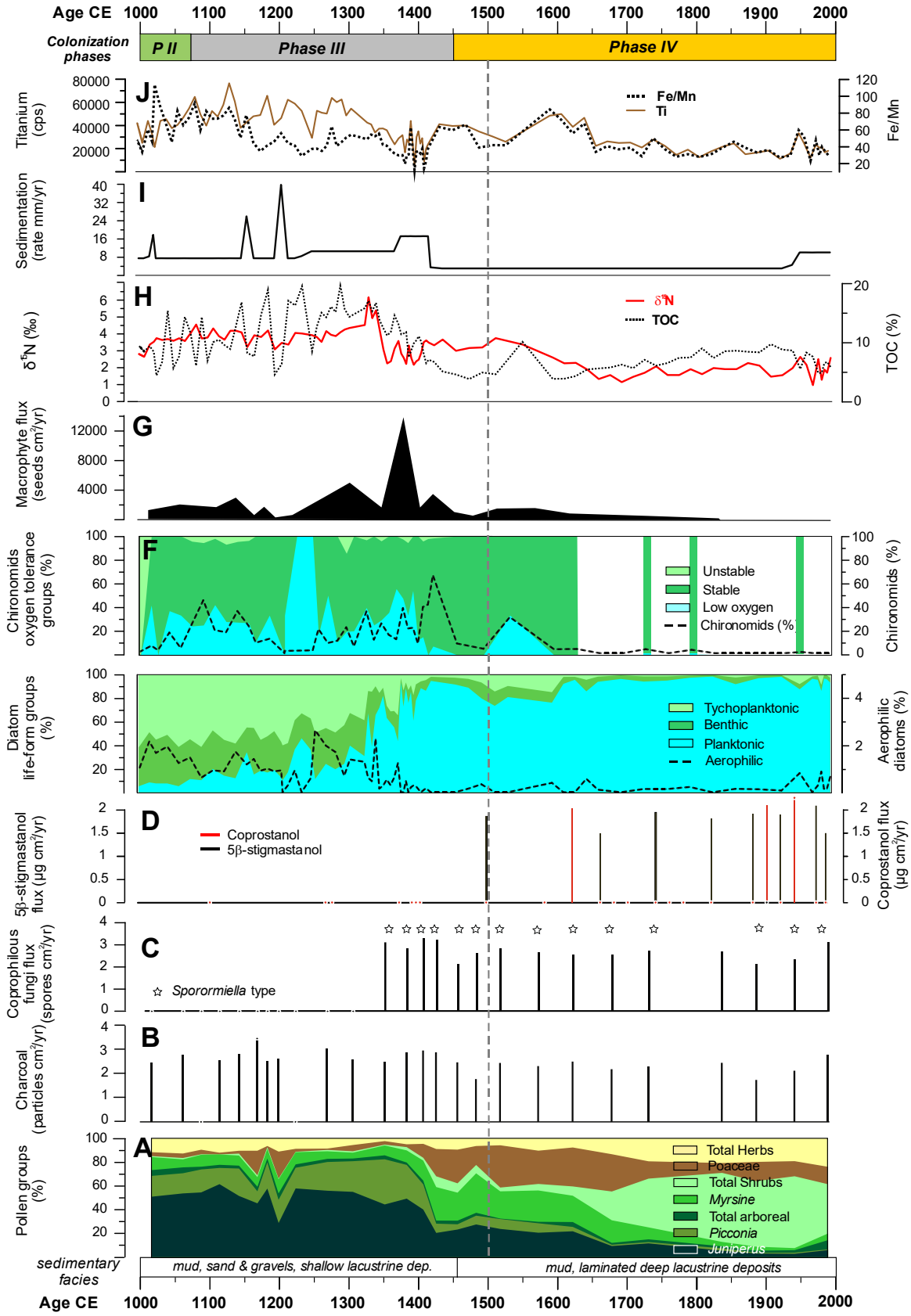
Age CE
1000
1100
1200
1300
1400
1500
1600
1700
1800
1900
2000
Colonization phases
P II
Phase III
Phase IV
J
Titanium (cps)
Fe/Mn
Ti
I
Sedimentation (rate mm/yr)
H
δ15N (‰)
TOC (%)
δ15N
TOC
G
Macrophyte flux (seeds cm2/yr)
F
Chironomids oxygen tolerance groups (%)
Unstable
Stable
Low oxygen
Chironomids (%)
Diatom life-form groups (%)
Tychoplanktonic
Benthic
Planktonic
Aerophilic
Aerophilic diatoms (%)
D
5β-stigmastanol flux (µg cm2/yr)
Coprostanol
5β-stigmastanol
Coprostanol flux (µg cm2/yr)
C
Coprophilous fungi flux (spores cm2/yr)
Sporormiella type
B
Charcoal (particles cm2/yr)
A
Pollen groups (%)
Total Herbs
Poaceae
Total Shrubs
Myrsine
Total arboreal
Picconia
Juniperus
sedimentary facies
mud, sand & gravels, shallow lacustrine dep.
mud, laminated deep lacustrine deposits

Fig. S2. Environmental evolution of Lake Funda (Flores Island) from 1000 to 1950CE. A) Pollen (%); B) Charcoal flux (particles. $cm^{-2}.y^{-1}$); C) Coprophilous fungi flux (spores. $cm^{-2}.y^{-1}$); D) Fecal sterol biomarkers 5β-stigmastanol flux (µg. $cm^{-2}.y^{-1}$) and coprostanol (5β-cholestan-3β-ol) E) Diatom life-forms groups (%) and aerophilic diatoms (%), F) Chironomid habitat associated (%) and chironomid head capsule flux ($cm^{-2}.y^{-1}$); G) Macrophyte influx (seeds $cm^{-2}.y^{-1}$) H) Nitrogen stable isotopes – δ15N (‰) and Total organic content – TOC (%); I) sedimentation rate ($mm^{-1}.y^{-1}$); J) Titanium (cps) and Fe/Mn ratio. Phases explanation (see main manuscript).

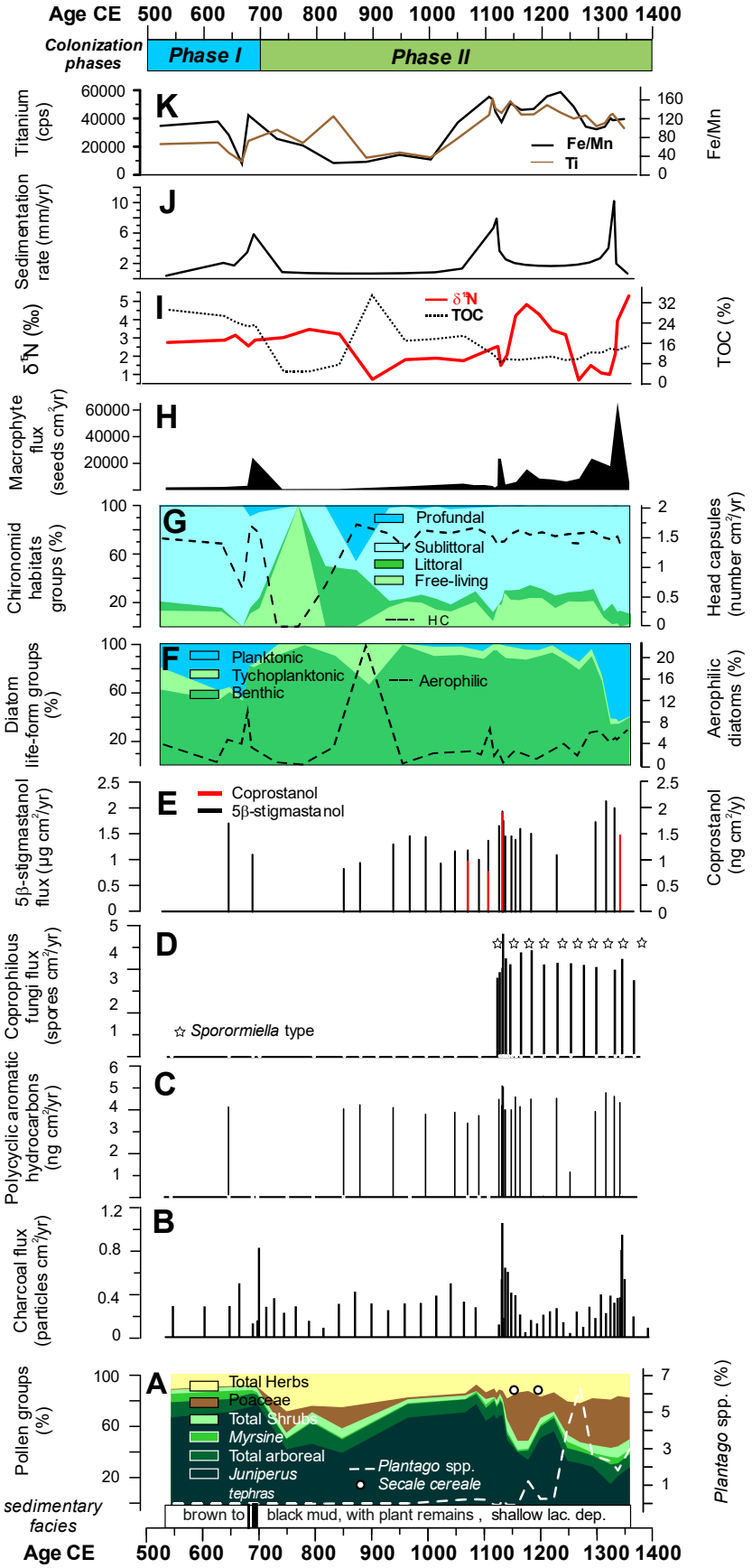
Age CE
500 600 700 800 900 1000 1100 1200 1300 1400
Colonization phases
Phase I
Phase II
K
Titanium (cps)
60000
40000
20000
0
Fe/Mn
Ti
160
120
80
40
0
Fe/Mn
J
Sedimentation rate (mm/yr)
10
6
2
I
δ15N (‰)
5
4
3
2
1
δ15N
TOC
32
24
16
8
0
TOC (%)
H
Macrophyte flux (seeds cm2yr)
60000
40000
20000
G
Chironomid habitats groups (%)
100
60
20
Profundal
Sublittoral
Littoral
Free-living
HC
2
1.5
1
0.5
0
Head capsules (number cm2/yr)
F
Diatom life-form groups (%)
Planktonic
Tychoplanktonic
Benthic
Aerophilic
20
16
12
8
4
0
Aerophilic diatoms (%)
E
5β-stigmastanol flux (µg cm2/yr)
2.5
2
1.5
1
0.5
0
Coprostanol
5β-stigmastanol
Coprostanol (ng cm2/y)
D
Coprophilous fungi flux (spores cm2/yr)
6
5
4
3
2
1
☆ Sporormiella type
C
Polycyclic aromatic hydrocarbons (ng cm2/yr)
B
Charcoal flux (particles cm2/yr)
1.2
0.8
0.4
0
A
Pollen groups (%)
Total Herbs
Poaceae
Total Shrubs
Myrsine
Total arboreal
Juniperus
tephras
Plantago spp.
Secale cereale
7
5
3
1
Plantago spp. (%)
sedimentary facies
brown to black mud, with plant remains , shallow lac. dep.
Age CE
500 600 700 800 900 1000 1100 1200 1300 1400

Fig. S3. Environmental evolution of Lake Peixinho (Pico Island) from 500 to 1800 CE. A) Pollen (%); B) Charcoal flux (particles. $cm^{-2}.y^{-1}$); C) Total pyrolytic PAHs flux (ng. $cm^{-2}.y^{-1}$); D) Coprophilous fungi flux (spores. $cm^{-2}.y^{-1}$); E) Fecal sterol biomarkers 5β-stigmastanol flux (µg. $cm^{-2}.y^{-1}$) and coprostanol (5β-cholestan-3β-ol) F) Diatom life-forms groups (%) and Aerophilic diatoms (%); G) Chironomid habitat associated (%) and chironomid head capsule flux ($cm^{-2}.y^{-1}$); H) Macrophyte influx (seeds $cm^{-2}.y^{-1}$); I)Nitrogen stable isotopes – δ15N (‰) and Total organic content – TOC (%); J) sedimentation rate ($mm\text{-}^{1}.y^{-1}$); K) Titanium (cps) and Fe/Mn ratio. Phases explanation (see main manuscript).

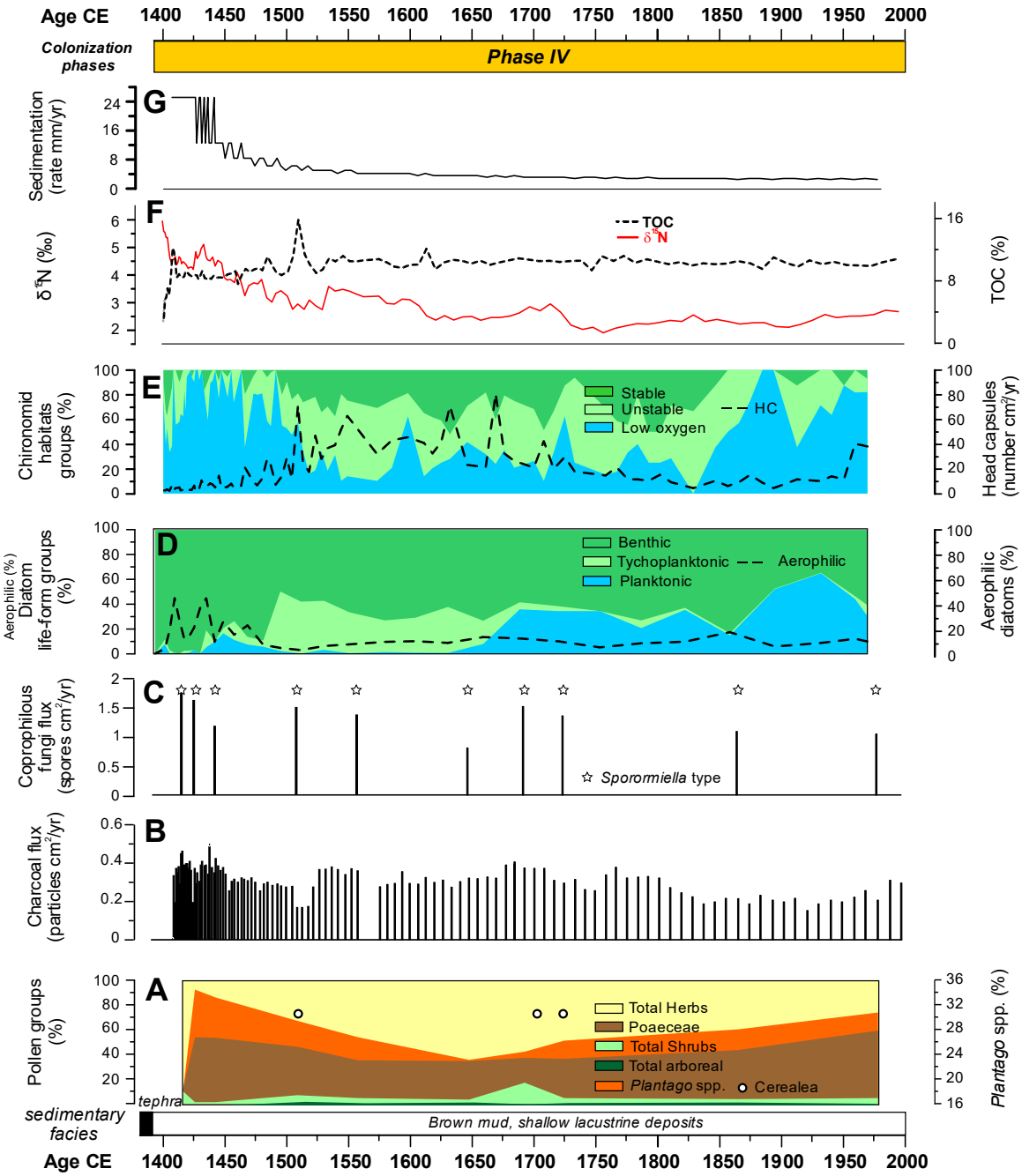

Fig. S4. Environmental evolution of Lake Ginjal (Terceira Island) from 1400 to 1800 CE. A) Pollen (%) and *Plantago* spp. (%); B) Charcoal flux (particles. $cm^{-2}.y^{-1}$); C) Coprophilous fungi flux (spores. $cm^{-2}.y^{-1}$); D) Diatom life-forms groups (%) and aerophilic diatoms (%), E) Chironomid habitat associated (%) and chironomid head capsule flux ($cm^{-2}.y^{-1}$); F) Nitrogen stable isotopes – δ15N (‰) and Total organic content – TOC (%); G) Sedimentation rate ($mm\text{-}^{1}.y^{-1}$). Phases explanation (see main manuscript).

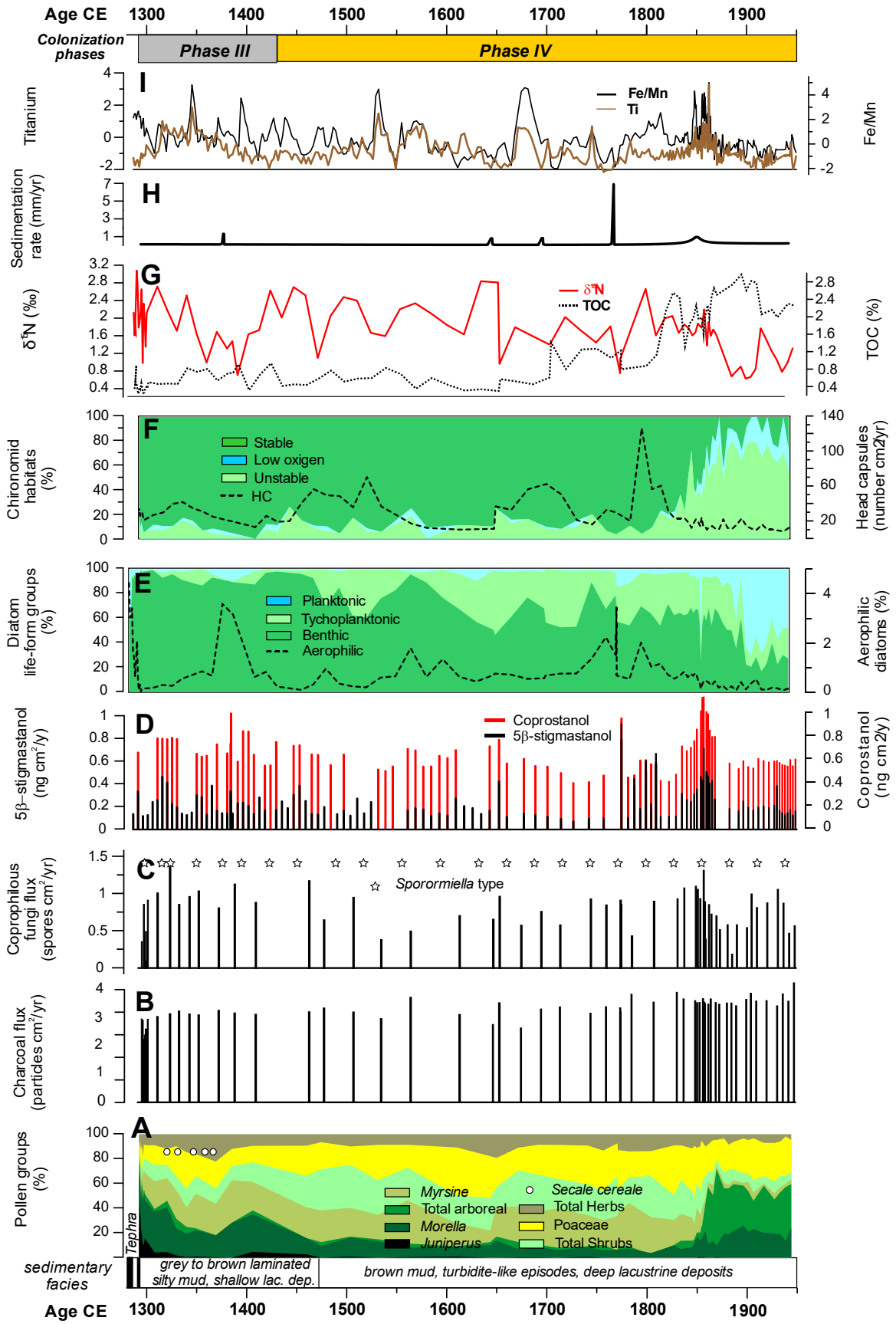
Age CE
1300
1400
1500
1600
1700
1800
1900
Colonization phases
Phase III
Phase IV
I
Titanium
Fe/Mn
Ti
Fe/Mn
H
Sedimentation rate (mm/yr)
G
δ15N (‰)
δ15N
TOC
TOC (%)
F
Chironomid habitats (%)
Stable
Low oxigen
Unstable
HC
Head capsules (number cm2yr)
E
Diatom life-form groups (%)
Planktonic
Tychoplanktonic
Benthic
Aerophilic
Aerophilic diatoms (%)
D
5β–stigmastanol (ng cm2/y)
Coprostanol
5β-stigmastanol
Coprostanol (ng cm2y)
C
Coprophilous fungi flux (spores cm2/yr)
Sporormiella type
B
Charcoal flux (particles cm2/yr)
A
Pollen groups (%)
Tephra
Myrsine
Total arboreal
Morella
Juniperus
Secale cereale
Total Herbs
Poaceae
Total Shrubs
sedimentary facies
grey to brown laminated silty mud, shallow lac. dep.
brown mud, turbidite-like episodes, deep lacustrine deposits

Fig. S5. Environmental evolution of Lake Azul (São Miguel Island) from 1280 to 1800 CE. A) Pollen (%); B) Charcoal flux (particles. $cm^{-2}.y^{-1}$); C) Coprophilous fungi flux (spores. $cm^{-2}.y^{-1}$); D) Fecal sterol biomarkers 5β-stigmastanol flux (ng. $cm^{-2}.y^{-1}$) and coprostanol (5β-cholestan-3β-ol) E) Diatom life-forms groups (%) and aerophilic diatoms (%); F) Chironomid habitat associated (%) and chironomid head capsule flux ($cm^{-2}.y^{-1}$); G) Nitrogen stable isotopes – δ15N (‰) and Total organic content – TOC (%); H) Sedimentation rate ($mm\text{-}^{1}.y^{-1}$); I) Titanium (cps) and Fe/Mn ratio. Phases explanation (see main manuscript).

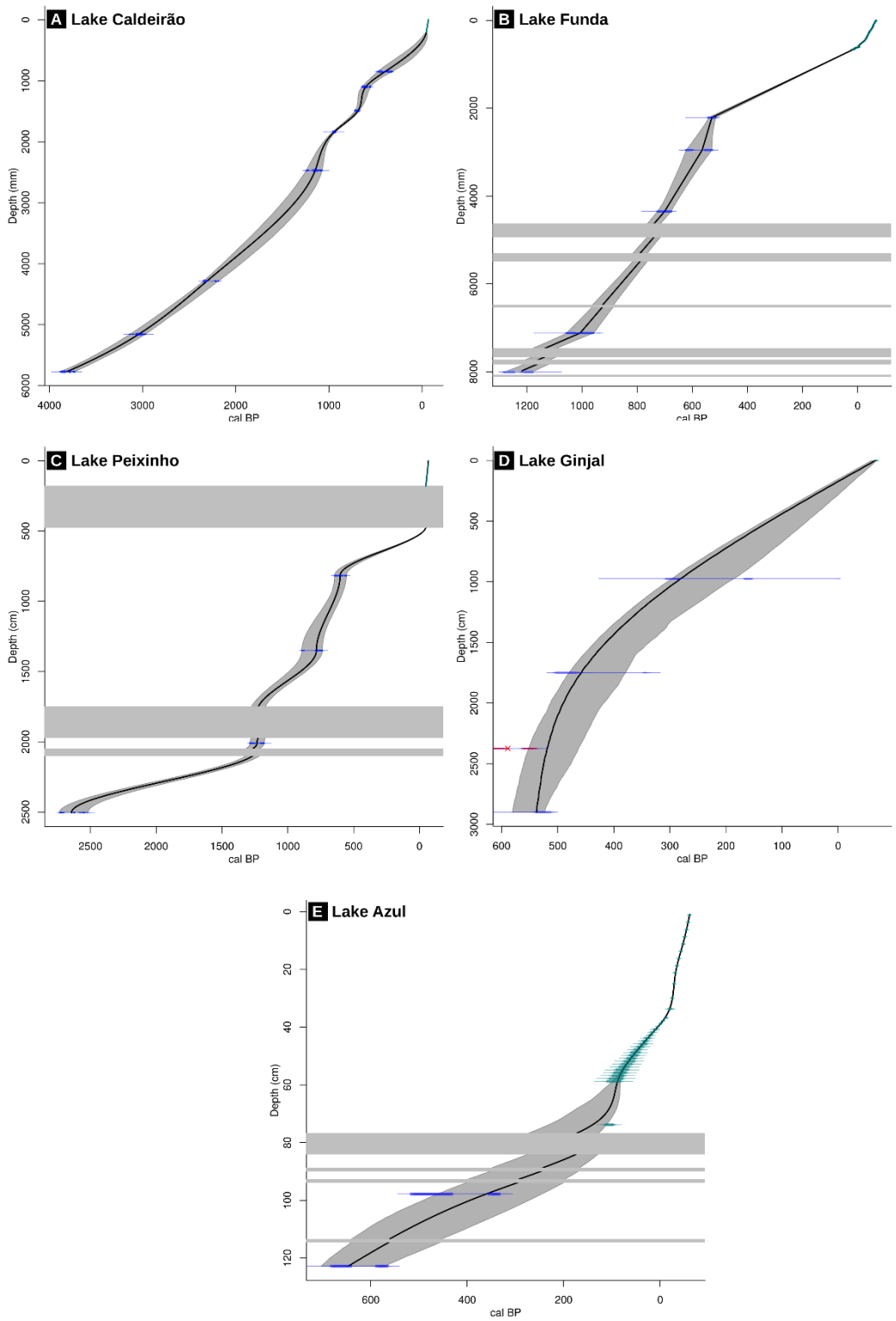
A Lake Caldeirão
Depth (mm)
cal BP
B Lake Funda
Depth (mm)
cal BP
C Lake Peixinho
Depth (cm)
cal BP
D Lake Ginjal
Depth (cm)
cal BP
E Lake Azul
Depth (cm)
cal BP

Fig. S6. Age-depth models of Lakes Caldeirão (A – top left), Funda (B – top right), Peixinho (C – middle left), Ginjal (D – middle right), and Azul (E – bottom center). All models were built using the R clam package version 2.3.9 (Blaauw, 2021), which uses the latest Intcal20 calibration curve. Horizontal gray bands denote the stratigraphic position of both instantaneous flood events (Lakes Azul, Funda, and the uppermost event of Peixinho) and volcanic tephras (lower two bands of Lake Peixinho). In green, the samples whose age was derived from the ^{210}Pb and ^{137}Cs profiles, in blue the radiocarbon dates used in the age-depth model construction, and in red the radiocarbon dates discarded. The confidence interval for the Lake Caldeirao age-depth model ranges between 1.5 and 124 years while for Lake Funda oscillates between 1 and 50 years, for Lake Peixinho fluctuates between 1 and 110 years, for Lake Ginja between 10 and 112 years, and finally, for Lake Azul between 1.4 and 223 years. Radiocarbon results employed to build these chronological models are in Table S2. Some radiocarbon dates were finally excluded of the final age-depth models due to inconsistent results. Most of these inconsistencies were related to the proximity of the dated material to allochthonous coarse terrigenous sediments (see the Records chronology section for further details).

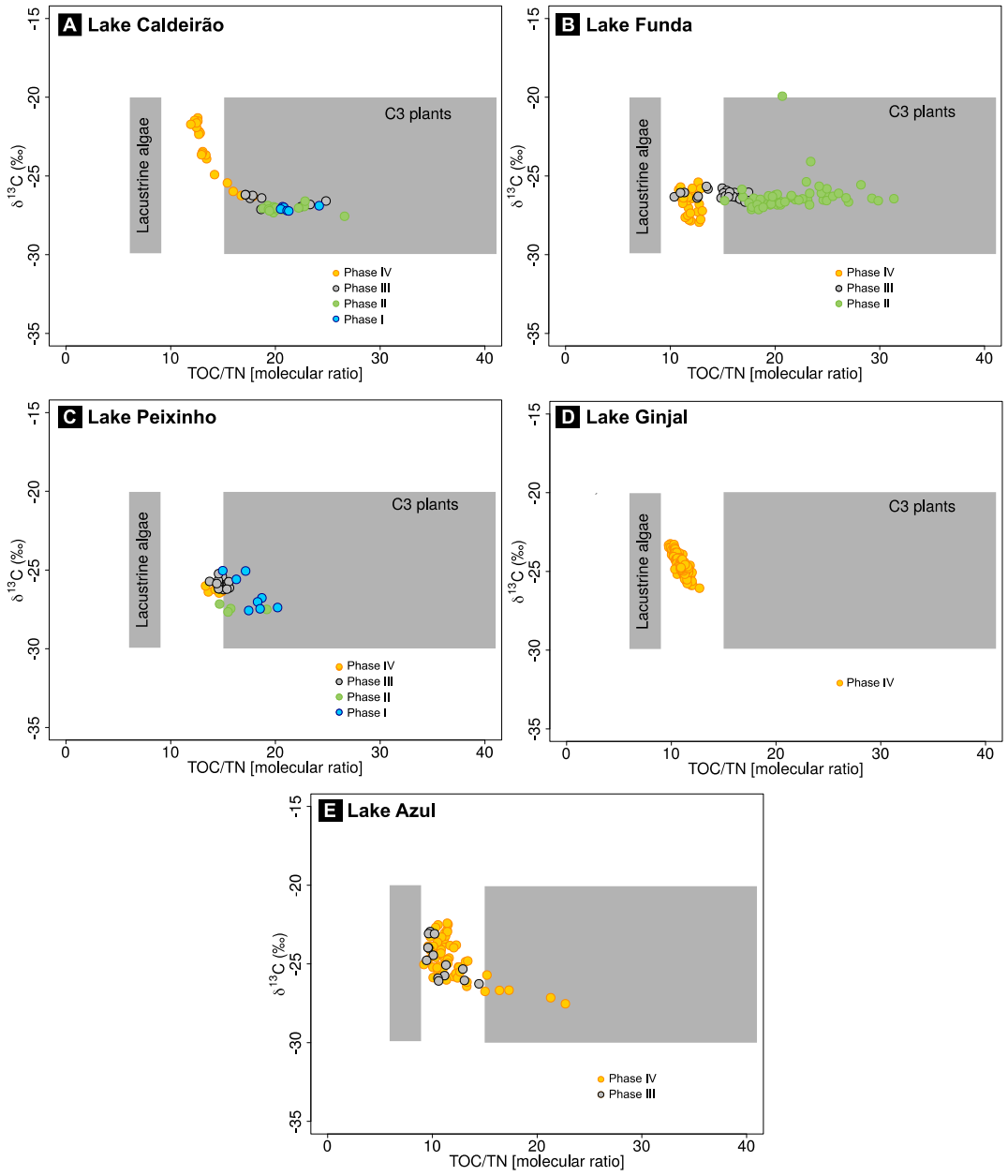

Fig. S7. Change in bulk organic matter content according to the three defined phases of anthropogenic impact compared to the "Pre-settlement phase". Western group A) Lake Caldeirão (Corvo Island); B) Lake Funda (Flores Island); Central group C) Lake Peixinho (Pico Island); D) Lake Ginjal (Terceira Island) and Eastern group E) Lake Azul (São Miguel Island). Changes in TOC/TN were interpreted in terms of allochthonous (vegetal cover debris) versus autochthonous (algal in-lake) sources while $\delta^{13}C$ was employed as one of the lake trophic status indicator (See the detailed climate and environmental reconstructions of the five lakes explained in the section "Environmental and climatic evolution of Lakes Caldeirão, Funda, Peixinho, Ginjal, and Azul" for further details).

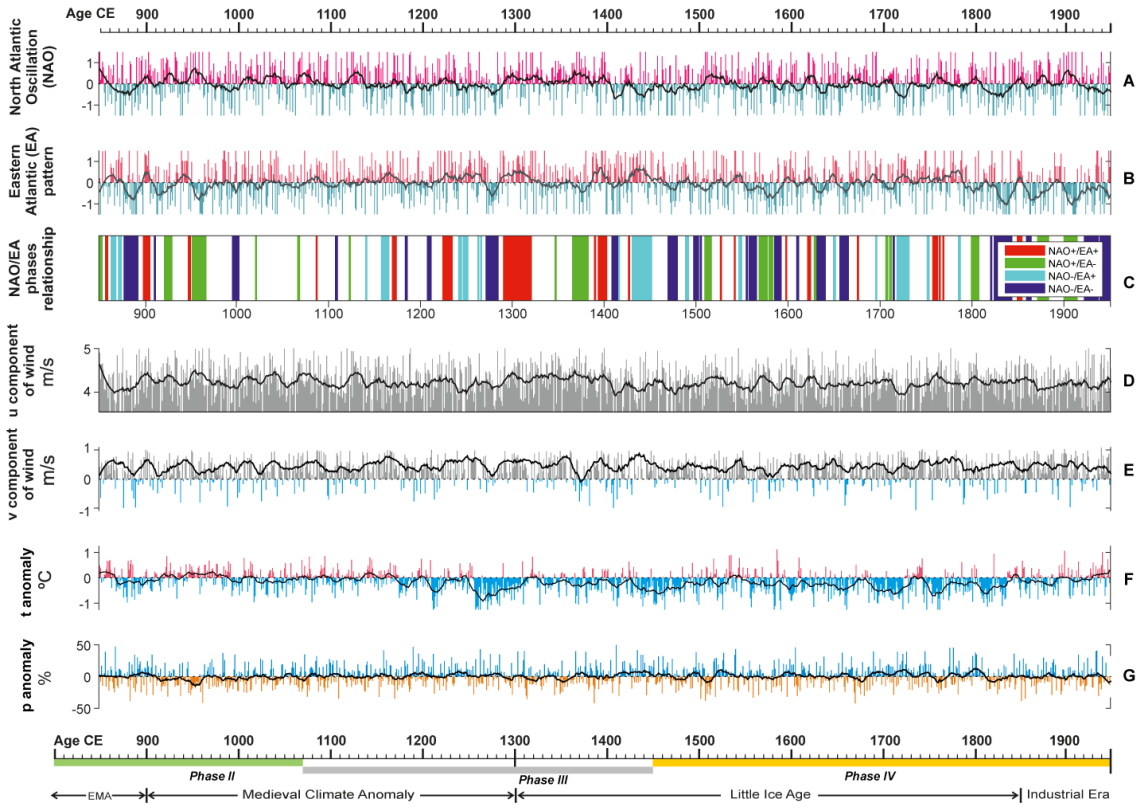

Fig. S8. (a) Extended winter (Oct-Mar) simulated NAO values between 850 and 1950 CE. The black line indicates a 30-year smoothing filter. (b) Extended winter simulated EA values between 850 and 1950 CE. The black line indicates a 30-year smoothing filter. (c) 30-years combinations of NAO and EA. (d) Extended winter simulated U-wind component between 850 and 1950 CE for the Azores Archipelago (0.95º X 1.25º grid). The black line indicates a 30-year smoothing filter. (e) Extended winter simulated V-wind component anomalies (computed for 850-1950 CE) between 850 and 1450 CE for the Azores Archipelago (0.95º X 1.25º grid). The black line indicates a 30-year smoothing filter. (f) Extended winter simulated temperature anomalies (computed for 850-1800 CE) between 850 and 1950 CE for the Azores Archipelago (0.95º X 1.25º grid). The black line indicates a 30-year smoothing filter. (g) Extended winter simulated precipitation anomalies (computed for 850-1950 CE) between 850 and 1950 CE for the Azores Archipelago (0.95º X 1.25º grid). The black line indicates a 30-year smoothing filter. Note that human activity phases and main North Atlantic climatic stages are indicated in the bottom timeline.

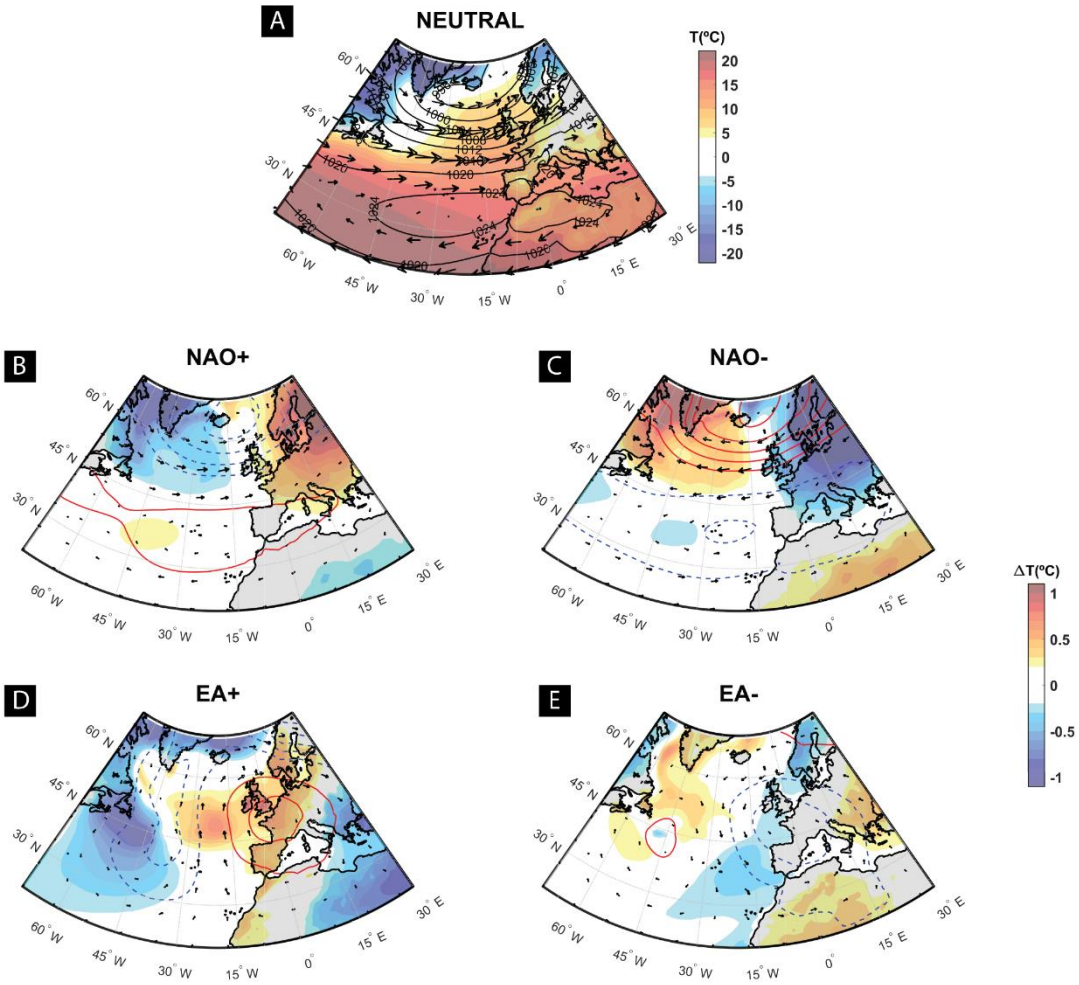

Fig. S9. Average anomalies for MSLP (blue/red lines), 2 m temperature (shading), and 925 hPa horizontal wind (vectors) for the combinations between concurrent positive/negative phases of the NAO and EA during 1901-2000 extended winters (October-March). (a) positive NAO and EA. (b) positive NAO and negative EA. (c) negative NAO and positive EA. (d) negative NAO and EA.

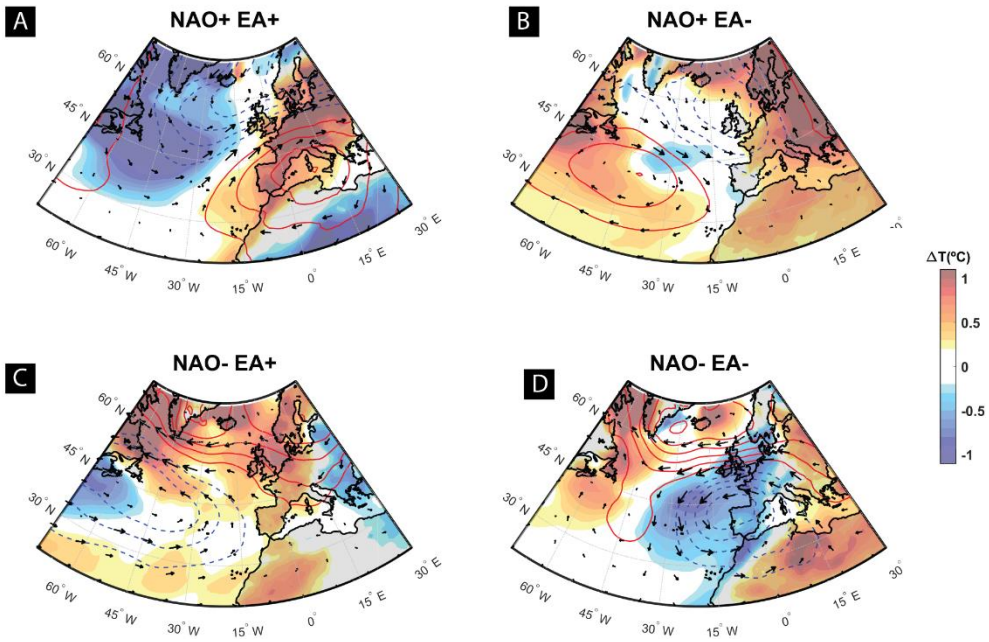

Fig. S10. Average anomalies for MSLP (blue/red lines), 2 m temperature (shading), and 925 hPa horizontal wind (vectors) for the combinations between concurrent positive/negative phases of the NAO and EA during 1901-2000 extended winters (October-March). (a) positive NAO and EA. (b) positive NAO and negative EA. (c) negative NAO and positive EA. (d) negative NAO and EA.

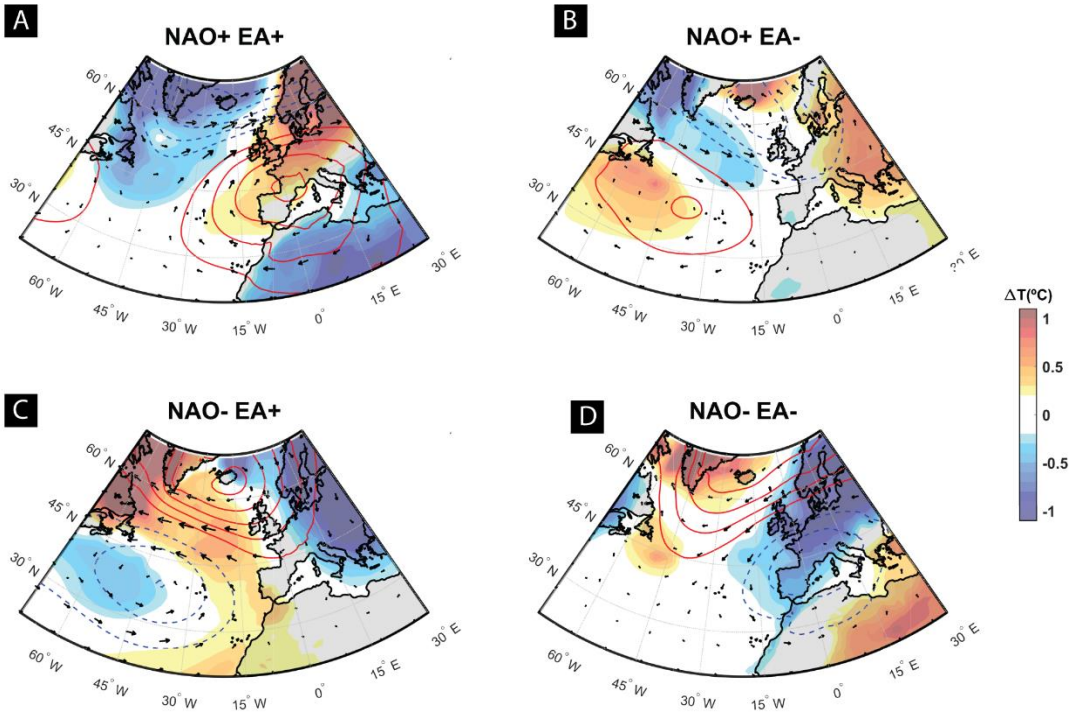

Fig. S11. Average anomalies for MSLP (blue/red lines), 2 m temperature (shading), and 925 hPa horizontal wind (vectors), for the combinations between concurrent positive/negative phases of the NAO and EA during 850 – 1450 CE period. (a) positive NAO and EA. (b) positive NAO and negative EA. (c) negative NAO and positive EA. (d) negative NAO and EA.

Tables

Table S1. Summary of the studied proxies and their sampling resolution in millimetres (mm) per lake. (–) indicates proxy method not used on a core and (X) indicates use of this dating method on a core.

Proxy Lake	Lake Funda	Lake Peixinho	Lake Ginjal	Lake Caldeirão	Lake Azul
X-Ray Fluorescence (XRF)	2	2	–	2	2
Bulk organic matter	50	40	25	50	10
Pollen	50-100	40-80	50	100	20
Plant macrorests	–	–	–	20	–
Macro-charcoal	–	40	25	50	–
Diatoms	100	40	20	50	20
Chironomids	100	40	20	50	10
Sterols	50	40	20	50	5
^{14}C AMS dates	X	X	X	X	X
^{210}Pb profile	X	X	–	X	X
^{137}Cs profile	X	X	–	–	X

Table S2. Radiocarbon dates of the sedimentary sequences, including laboratory code (UCIMAS- University of California; ULA – University of Laval and Beta – Beta Analytic), sample description, sample ID, collected depth cm), pre-treatment, fraction modern values F14C, per mil depletion or enrichment D14C, uncalibrated 14C ages and 14C calibrated ages

Laboratory code		Sample description	Sample ID	Depth (cm)	Pre-treatment	F ^{14}C	D ^{14}C	^{14}C age (yrs BP)	2-σ cal. ^{14}C age (yrs BP)
			Lake Caldeirão (Corvo Island)						
UCIAMS-203216	ULA 7752	Pollen concentrate	CL1703-01-78	85	HCl	0.9573 ± 0.0023	-42.7 ± 2.3	350 ± 20	390 $^{+10}_{-70}$
UCIAMS-230042	ULA-8880	Pollen concentrate	CL19-02G	110	HCl-NaOH-HCl	0.9277 ± 0.0015	-72.3 ± 1.5	605 ± 15	604 $^{+40}_{-20}$
UCIAMS-212644	ULA-8250	Pollen concentrate	CL1703-01-149	149	HCl	0.9089 ± 0.0015	-91.1 ± 1.5	765 ± 15	688 $^{+20}_{-20}$
UCIAMS-230043	ULA-8881	Pollen concentrate	CL19-02G	190	HCl-NaOH-HCl	0.8705 ± 0.0015	-129.5 ± 1.5	1115 ± 15	1015 $^{+45}_{-40}$
UCIAMS-203215	ULA-7751	Pollen concentrate	CL1703-02-65	247	HCl-NaOH-HCl	0.8586 ± 0.0018	-141.4 ± 1.8	1225 ± 20	1150 $^{+30}_{-80}$
UCIAMS-215536	ULA-8356	Pollen concentrate	CL1703-03-66	428.4	HCl-NaOH-HCl	0.7517 ± 0.0014	-248.3 ± 1.4	2295 ± 20	2335 $^{+15}_{-25}$
UCIAMS-215537	ULA-8357	Pollen concentrate	CL1703-03-144	515.5	HCl-NaOH-HCl	0.6966 ± 0.0012	-303.4 ± 1.2	2905 ± 15	3035 $^{+40}_{-70}$
UCIAMS-203208	ULA-7750	Pollen concentrate	CL1703-04-28	577	HCl-NaOH-HCl	0.6437 ± 0.015	-356.3 ± 1.5	3540 ± 20	3840 $^{+50}_{-20}$
			Lake Funda (Flores Island)						
UCIAMS-203206	ULA-7746	Pollen concentrate	FN1702-01-52.8	60.8	HCl-NaOH-HCl	1.0097 ± 0.0025	9.7 ± 2.5	Modern	1955.6 $^{+0.3}_{-0.3}$
UCIAMS-170194	ULA-5787	Pollen concentrate	FN1702-01-154	162	none	0.9363 ± 0.0017	-63.7 ± 1.7	530 ± 15	537 $^{+10}_{-10}$
UCIAMS-203213	ULA-7747	Pollen concentrate	FN1702-01-160	168	HCl-NaOH-HCl	0.8359 ± 0.0019	-164.1 ± 1.9	1440 ± 20	1330 $^{+40}_{-30}$
UCIAMS-200963	ULA-7657	Pollen concentrate	FN1702-02-34	221.2	HCl-NaOH-HCl	0.9385 ± 0.0017	-61.5 ± 1.7	510 ± 15	530 $^{+10}_{-10}$
UCIAMS-203205	ULA-7745	Pollen concentrate	FN1702-02-108	295.2	HCl-NaOH-HCl	0.9338 ± 0.0022	-66.2 ± 2.2	550 ± 20	550 $^{+80}_{-50}$
UCIAMS-203204	ULA-7744	Pollen concentrate	FN1702-03-67	435	HCl-NaOH-HCl	0.9067 ± 0.0022	-93.3 ± 2.2	785 ± 20	700 $^{+30}_{-20}$
UCIAMS-203202	ULA-7738	Pollen concentrate	FN1702-04-47	624	HCl-NaOH-HCl	0.8461 ± 0.0020	-153.9 ± 2.0	1340 ± 20	1280 $^{+20}_{-20}$
UCIAMS-203203	ULA-7739	Pollen concentrate	FN1702-04-135	712	HCl-NaOH-HCl	0.8722 ± 0.0020	-127.8 ± 2.0	1100 ± 20	1000 $^{+60}_{-40}$
UCIAMS-203201	ULA-7737	Pollen concentrate	FN1702-05-73	801	HCl-NaOH-HCl	0.8508 ± 0.0020	-149.2 ± 2.0	1300 ± 20	1250 $^{+40}_{-20}$
UCIAMS-200961	ULA-7655	Pollen concentrate	FN1702-06-71	992	HCl-NaOH-HCl	0.8834 ± 0.0018	-116.6 ± 1.8	995 ± 20	930 $^{+30}_{-30}$
			Lake Peixinho (Pico Island)						
UCIAMS-167858	ULA-5708	Pollen concentrate	PEX171B-01-36	47.6	HCl	0.9454 ± 0.0018	-54.6 ± 1.8	450 ± 20	510 $^{+20}_{-20}$
UCIAMS-167856	ULA-5705	Pollen concentrate	PEX171A-01-81	81.7	none	0.9264 ± 0.0021	-73.6 ± 2.1	615 ± 20	600 $^{+50}_{-10}$
UCIAMS-170195	ULA-5788	Pollen concentrate	PEX171A-01-135	135	none	0.8950 ± 0.0016	-105.0 ± 1.6	890 ± 15	790 $^{+10}_{-50}$
UCIAMS-167857	ULA-5707	Pollen concentrate	PEX171Csup-53	201	none	0.8491 ± 0.0021	-150.9 ± 2.1	1315 ± 20	1270 $^{+20}_{-30}$
UCIAMS-167869	ULA-5719	Pollen concentrate	PEX171Csup-104	250.4	HCl	0.7288 ± 0.0017	-271.2 ± 1.7	2540 ± 20	2715 $^{+30}_{-20}$
			Lake Ginjal (Terceira Island)						
UCIAMS-215539	ULA-8359	Pollen concentrate	GN-01 M1 40	41.2	HCl	0.9653 ± 0.0017	-34.7 ± 1.7	285 ± 15	385 $^{+50}_{-5}$
UCIAMS-211262	ULA-8211	Pollen concentrate	GW-01-02 47.5-50	97.5	HCl	0.9698 ± 0.0017	-30.2 ± 1.7	245 ± 15	295 $^{+10}_{-10}$

UCIAMS-211261	ULA-8210	Pollen concentrate	GW-01-04 25-27.5	175	none	0.9516 ± 0.0020	-48.4 ± 2.0	400 ± 20	485 $^{+25}_{-35}$
UCIAMS-211263	ULA-8212	Pollen concentrate	GW-01-05 37.5-40	275	HCl	0.9306 ± 0.0021	-69.4 ± 2.1	580 ± 20	610 $^{+30}_{-20}$
UCIAMS-215540	ULA-8360	Pollen concentrate	GN M6 25 290	238.2	HCl-NaOH-HCl	0.9392 ± 0.0016	-60.8 ± 1.6	505 ± 15	530 $^{+10}_{-20}$
			Lake Azul (São Miguel Island)						
Beta-316595		Macrorest	AZ11-02-46	82.8	alkali	–	–	200 ± 30	180 $^{+40}_{-40}$
Beta-331408		Macrorest	AZ11-02-61	97.8	alkali	–	–	420 ± 30	490 $^{+30}_{-55}$
Beta-331409		Macrorest	AZ11-02-86	122.8	alkali	–	–	690 ± 30	660 $^{+20}_{-20}$

SI References

1. R. S. Ramalho, *et al.*, Emergence and evolution of Santa Maria Island (Azores) - The conundrum of uplifted islands revisited. *Bull. Geol. Soc. Am.* **129**, 372–391 (2017).
2. A. C. G. Costa, A. Hildenbrand, F. O. Marques, A. L. R. Sibrant, A. Santos de Campos, Catastrophic flank collapses and slumping in Pico Island during the last 130 kyr (Pico-Faial ridge, Azores Triple Junction). *J. Volcanol. Geotherm. Res.* **302**, 33–46 (2015).
3. A. Hernández, *et al.*, The influences of the AMO and NAO on the sedimentary infill in an Azores Archipelago lake since ca. 1350 CE. *Glob. Planet. Change* **154**, 61–74 (2017).
4. A. Hernández, *et al.*, New Azores archipelago daily precipitation dataset and its links with large-scale modes of climate variability. *Int. J. Climatol.* **36**, 4439–4454 (2016).
5. D. L. Volkov, L. Fu, On the reasons for the formation and variability of the Azores current. *J. Phys. Oceanogr.* **40**, 2197–2220 (2010).
6. J. W. Hurrell, Y. Kushnir, G. Ottersen, M. Visbeck, An Overview of the North Atlantic Oscillation. *North Atl. Oscil. Clim. Significance Environ. Impact*, 1–35 (2003).
7. T. E. Cropper, E. Hanna, An analysis of the climate of Macaronesia, 1865–2012. *Int. J. Climatol.* **34**, 604–622 (2014).
8. A. Hernández, *et al.*, A 2,000-year Bayesian NAO reconstruction from the Iberian Peninsula. *Sci. Rep.* **10**, 14961 (2020).
9. S. E. Connor, *et al.*, The ecological impact of oceanic island colonization – a palaeoecological perspective from the Azores. *J. Biogeogr.*, 1–17 (2012).
10. J. F. N. van Leeuwen, *et al.*, Native or introduced? Fossil pollen and spores may say. An example from the Azores Island. *Neobiota* **6**, 27–34 (2005).
11. C. A. Góis-Marques, *et al.*, The loss of a unique palaeobotanical site in Terceira island within the Azores UNESCO global geopark (Portugal). *Geoheritage* **11**, 1817–1825 (2019).
12. C. A. Góis-Marques, L. de Nascimento, M. Menezes de Sequeira, J. M. Fernández-Palacios, J. Madeira, The Quaternary plant fossil record from the volcanic Azores Archipelago (Portugal, North Atlantic Ocean): a review. *Hist. Biol.* **31**, 1267–1283 (2019).
13. J. M. Moreira, *Alguns aspectos de intervenção humana na evolução da paisagem da ilha de S. Miguel (Açores)* (Serviço Nacional de Parques, Reservas e Conservação da Natureza, 1987).
14. G. Frutuoso, *Livro Sexto das Saudades da Terra*, Instituto (1978).
15. R. D. Gregório, “Terra e fortuna nos primórdios da Ilha Terceira (1450-1550),” Universidade dos Açores. (2006).
16. G. Frutuoso, *Livro Quarto das Saudades da Terra* (Instituto Cultural de Ponta Delgada, 1981).
17. K. A. Triantis, *et al.*, Extinction debt on oceanic Islands. *Ecography* **33**, 285–294 (2010).
18. R. B. Elias, *et al.*, Natural zonal vegetation of the Azores Islands: Characterization and potential distribution. *Phytocoenologia* **46**, 107–123 (2016).
19. J. Porteiro, “Lagoas dos Açores: elementos de suporte ao planeamento integrado,” Universidade dos Açores, Ponta Delgada. (2000).
20. C. L. Pereira, *et al.*, Biogeography and lake morphometry drive diatom and chironomid assemblages’ composition in lacustrine surface sediments of oceanic islands. *Hydrobiologia* **730**, 93–112 (2014).

21. V. Gonçalves, “Contribuição do estudo das microalgas para a avaliação da qualidade ecológica das lagoas dos Açores: fitoplâncton e diatomáceas bentónicas,” University of the Azores, Ponta Delgada. (2008).

22. J. V. Cruz, *et al.*, Sete Cidades and Furnas lake eutrophication (São Miguel, Azores): Analysis of long-term monitoring data and remediation measures. *Sci. Total Environ.* **520**, 168–186 (2015).

23. A. C. Costa, *et al.*, Non-indigenous and Invasive Freshwater Species on the Atlantic Islands of the Azores Archipelago . *Front. Ecol. Evol.* **9**, 211 (2021).

24. M. G. Matias, *et al.*, Divergent trophic responses to biogeographic and environmental gradients. *Oikos* **126**, 101–110 (2017).

25. P. M. Raposeiro, A. M. Cruz, S. J. Hughes, A. C. Costa, Azorean freshwater invertebrates: Status, threats and biogeographic notes. *Limnetica* **31**, 13–22 (2012).

26. P. M. Raposeiro, A. Sáez, S. Giralt, A. C. Costa, V. Gonçalves, Causes of spatial distribution of subfossil diatom and chironomid assemblages in surface sediments of a remote deep island lake. *Hydrobiologia* **815**, 141–163 (2018).

27. M. R. Talbot, “Nitrogen isotopes in paleolimnology” in *Tracking Environmental Change Using Lake Sediments. Physical and Geochemical Methods*, J. P. Smol, H. J. B. Birks, W. M. Last, Eds. (Kluwer Academic Publishers, 2001), pp. 401–439.

28. K. D. Bennett, W. J. Willis, “Pollen” in *Tracking Environmental Change Using Lake Sediments, Terrestrial, Algal and Siliceous Indicators*, J. P. Smol, H. J. B. Birks, W. M. Last, Eds. (Kluwer, 2001), pp. 5–32.

29. R. B. Moore, *Geology of the three Late Quaternary Stratovolcanoes on São Miguel, Azores* (US Geological Survey Bulletin, 1991).

30. M. Reille, *Pollen et Spores d’Europe et d’Afrique du Nord* (Laboratoire de Botanique Historique et Palynologie).

31. D. Demske, P. E. Tarasov, T. Nakagawa, S. P. Members, Atlas of pollen, spores and further non-pollen palynomorphs recorded in the glacial-interglacial Ia Quaternary sediments of lake Suigetsu, central Japan. *Quat. Int.* **290**–**291**, 164–238 (2013).

32. B. van Geel, A. Aptroot, Fossil ascomycetes in Quaternary deposits. *Nov. Hedwigia* **82**, 313–329 (2006).

33. B. van Geel, *et al.*, Diversity and ecology of tropical African fungal spores from a 25,000-year palaeoenvironmental record in southeastern Kenya. *Rev. Palaeobot. Palynol.* **164**, 174–190 (2011).

34. C. Cugny, F. Mazier, D. Galop, Modern and fossil non-pollen palynomorphs from the Basque mountains (western Pyrenees, France): the use of coprophilous fungi to reconstruct pastoral activity. *Veg. Hist. Archaeobot.* **19**, 391–408 (2010).

35. E. Montoya, V. Rull, T. Vegas-Vilarrúbia, Non-pollen palynomorph studies in the Neotropics: the case of Venezuela. *Rev. Palaeobot. Palynol.* **186**, 102–130 (2012).

36. C. Joly, L. Barillé, M. Barreau, A. Mancheron, L. Visset, Grain and annulus diameter as criteria for distinguishing pollen grains of cereals from wild grasses. *Rev. Palaeobot. Palynol.* **146**, 221–233 (2007).

37. H.-J. Beug, *Leitfaden der Pollesbestimmung für Mitteleuropa und angrenzende Gebiete* (2004).

38. V. Rull, A note on pollen counting in palaeoecology. *Pollen Spores* **29**, 471–480 (1987).

39. V. Rull, *et al.*, Vegetation and landscape dynamics under natural and anthropogenic forcing on the Azores Islands: A 700-year pollen record from the São Miguel Island. *Quat.*

Sci. Rev. **159**, 155–168 (2017).

40. G. Berggren, *Atlas of seeds. Part 2. Cyperaceae* (Swedish Museum of Natural History, 1964).

41. G. Berggren, *Atlas of seeds. Part 3. Salicaceae-Cruciferae* (Swedish Museum of Natural History, 1981).

42. W. Beijerinck, *Zadenatlas der Nederlandsche flora:: ten behoeve van de botanie, palaeontologie, bodemcultuur en warenkennis* (Backhuys & Meesters, 1976).

43. G. Grosse-Brauckmann, Über pflanzliche Makrofossilien mitteleuropäischer Torfe. II. Weitere Reste (Früchte und Samen, Moose u.a.) und ihre Bestimmungsmöglichkeiten. *Telma* **4**, 51–117 (1974).

44. G. Grosse-Brauckmann, B. Streit, Pflanzliche Makrofossilien mitteleuropäischer Torfe. III. Früchte, Samen und einige Gewebe (Fotos von fossilen Pflanzenresten). *Telma* **22**, 53–102 (1992).

45. G. Grosse-Brauckmann, Über pflanzliche Makrofossilien mitteleuropäischer Torfe. I. Gewebereste krautiger Pflanzen und ihre Merkmale. *Telma* **2**, 19–55 (1972).

46. D. Mauquoy, B. Hughes PDM van Geel, A protocol for plant macrofossil analysis of peat deposits. *Mires Peat* **7**, 1–5 (2010).

47. I. Renberg, A procedure for preparing large sets of diatom slides from sediment cores. *J. Paleolimnol.* **4**, 87–90 (1990).

48. K. Krammer, H. Lange-Bertalot, *Bacillariophyceae. 2/5: English and French translation of the keys*, H. Ettl, Ed. (G. Fisher Verlag, 2000).

49. K. Krammer, H. Lange-Bertalot, Bacillariophyceae.

50. K. Krammer, H. Lange-Bertalot, *Bacillariophyceae. 2/3: Centrales, Fragilariaceae, Eunotiaceae*, H. Ettl, Ed. (G. Fisher Verlag, 1991).

51. K. Krammer, H. Lange-Bertalot, *Bacillariophyceae. 2/4: Achnanthaceae*, H. Ettl, Ed. (G. Fisher Verlag, 1991).

52. K. Krammer, H. Lange-Bertalot, *Bacillariophyceae 2/2 Bacillariaceae, Epithemiaceae, Surirellaceae.*, H. Ettl, Ed. (G. Fisher Verlag, 1988).

53. H. Lange-Bertalot, Diatoms of the European Inland Waters and comparable Habitats.

54. J. Prygiel, M. Coste, *Guide Méthodologique pour la mise en oeuvre de l'Indice Biologique Diatomées* (Agences de l'Eau, 2000).

55. V. Gonçalves, H. Marques, A. Fonseca, "Lista das Diatomáceas (Bacillariophyta)" in *Listagem Dos Organismos Terrestres e Marinhos Dos A{c}cores*, P. A. V Borges, *et al.*, Eds. (Princípia, 2010), pp. 81–97.

56. J. A. Wolin, J. R. Stone, "Diatoms as indicators of water-level change in freshwater lakes" in *The Diatoms Applications to Environmental and Earth Sciences*, E. F. Stoermer, J. P. Smol, Eds. (Cambridge University Press, 2010), pp. 174–185.

57. J. R. Johansen, "Diatoms of aerial habitats" in *The Diatoms Applications to Environmental and Earth Sciences*, E. F. Stoermer, J. P. Smol, Eds. (Cambridge University Press, 2010), pp. 465–472.

58. S. J. Brooks, P. G. Langdon, O. Heiri, *The Identificiation and Use of Palaeartic Chironomidae Larvae in Palaeoecology* (Quarternary Research Association, 2007).

59. S. R. Q. Serra, M. A. S. Graça, S. Dolédec, M. J. Feio, Discriminating permanent from temporary rivers with traits of chironomid genera. *Int. J. Limnol.* **53**, 161–174 (2017).

60. V. Rull, N. D. Stansell, E. Montoya, M. Bezada, M. B. Abbott, Palynological signal of the

Younger Dryas in the tropical Venezuelan andes. *Quat. Sci. Rev.* **29**, 3045–3056 (2010).

61. P. J. Reimer, *et al.*, The IntCal13 Northern Hemisphere radiocarbon age calibration curve (0-55 cal kBP. *Radiocarbon* **62**, 725–757 (2020).

62. J. A. Sanchez-Cabeza, P. Masqué, I. Ani-Ragolta, Lead-210 and Po-210 analysis in sediments and soils by microwave acid digestion. *J. Radioanal. Nucl. Chem.* **227**, 19–22 (1998).

63. A. C. Ruiz-Fernández, C. Hillaire-Marcel, ^{210}Pb-derived ages for the reconstruction of terrestrial contaminant history into the Mexican Pacific coast: Potential and limitations. *Mar. Pollut. Bull.* **59**, 134–145 (2009).

64. W. W. Flynn, The determination of low levels of polonium-210 in environmental materials. *Anal. Chim. Acta* **43**, 221–227 (1968).

65. P. G. Appleby, F. Oldfield, The calculation of lead-210 dates assuming a constant rate of supply of unsupported 210Pb to the sediment. *Catena*, 1–8 (1978).

66. J. A. Sanchez-Cabeza, A. C. Ruiz-Fernández, ^{210}Pb sediment radiochronology: an integrated formulation and classification of dating models. *Geochim. Cosmochim. Acta* **82**, 183–200 (2012).

67. J. A. Robbins, “Geochemical and geophysical applications of radioactive lead” in *The Biogeochemistry of Lead in the Environment*, J. O. Nriagu, Ed. (Elsevier, 1978), pp. 285–393.

68. J. A. Sanchez-Cabeza, A. C. Ruiz-Fernández, J. F. Ontiveros-Cuadras, L. H. P. Bernal, C. Olid, Monte Carlo uncertainty calculation of 210Pb chronologies and accumulation rates of sediments and peat bogs. *Quat. Geochronol.* **23**, 80–93 (2014).

69. M. Blaauw, J. A. Christen, J. E. Vazquez, S. Goring, Clam - Classical Age-Depth Modelling of Cores from Deposits. *R Packag. version 2.3.7* (2020).

70. M. Blaauw, Methods and code for “classical” age-modelling of radiocarbon sequences. *Quat. Geochronol.* **5**, 512–518 (2010).

71. N. J. Abram, *et al.*, Early onset of industrial-era warming across the oceans and continents. *Nature* **536**, 411–418 (2016).

72. Q. Fu, L. Lin, J. Huang, S. Feng, A. Gettelman, Changes in terrestrial aridity for the period 850–2080 from the Community Earth System Model. *J. Geophys. Res. Atmos.* **121**, 2857–2873 (2016).

73. C. C. Raible, *et al.*, Tambora 1815 as a test case for high impact volcanic eruptions: Earth system effects. *WIREs Clim. Chang.* **7**, 569–589 (2016).

74. P. M. Sousa, *et al.*, North Atlantic integrated water vapor transport-from 850 to 2100 CE: Impacts on Western European rainfall. *J. Clim.* **33**, 263–279 (2020).

75. R. Zhang, *et al.*, A Review of the Role of the Atlantic Meridional Overturning Circulation in Atlantic Multidecadal Variability and Associated Climate Impacts. *Rev. Geophys.* **57**, 316–375 (2019).

76. M. P. King, E. Yu, J. Sillmann, Impact of strong and extreme El Niños on European hydroclimate. *Tellus A Dyn. Meteorol. Oceanogr.* **72**, 1–10 (2020).

77. T. J. Osborn, K. R. Briffa, S. F. B. Tett, P. D. Jones, R. M. Trigo, Evaluation of the North Atlantic Oscillation as simulated by a coupled climate model. *Clim. Dyn.* **15**, 685–702 (1999).

78. L. Comas-Bru, A. Hernández, Reconciling North Atlantic climate modes: revised monthly indices for the East Atlantic and the Scandinavian patterns beyond the 20th century. *Earth Syst. Sci. Data* **10**, 2329–2344 (2018).

79. D. Vázquez-Loureiro, *et al.*, Diatom-inferred ecological responses of an oceanic lake system to volcanism and anthropogenic perturbations since 1290 CE. *Palaeogeogr. Palaeoclimatol. Palaeoecol.* **534**, 109285 (2019).

80. R Core Team, R: A Language and Environment for Statistical Computing (2020).

81. P. A. Meyers, Applications of organic geochemistry to paleolimnological reconstructions: a summary of examples from the Laurentian Great Lakes. *Org. Geochem.* **34**, 261–289 (2003).

82. P. A. Meyers, Preservation of elemental and isotopic source identification of sedimentary organic matter. *Chem. Geol.* **114**, 289–302 (1994).

83. P. M. Raposeiro, *et al.*, Impact of the historical introduction of exotic fishes on the chironomid community of Lake Azul (Azores Islands). *Palaeogeogr. Palaeoecol.* **466**, 77–88 (2017).

84. H. Van Dam, A. Mertens, J. Sinkeldam, A coded checklist and ecological indicator values of freshwater diatoms from The Netherlands. *Netherl. J. Aquat. Ecol.* **28**, 117–133 (1994).

85. S. Naeher, A. Gilli, R. P. North, Y. Hamann, C. J. Schubert, Tracing bottom water oxygenation with sedimentary Mn/Fe ratios in Lake Zurich, Switzerland. *Chem. Geol.* **352**, 125–133 (2013).

86. M. E. Mann, *et al.*, Global signatures and dynamical origins of the Little Ice Age and Medieval Climate Anomaly. *Science* **326**, 1256–1260 (2009).